AD-A034 006 AIR FORCE INST OF TECH WRIGHT-PATTERSON AFB OHIO SCH--ETC F/G 20/5
AN EXPERIMENTAL INVESTIGATION OF THE RESONANT MODES OF A ROOFTO--ETC(U)
DEC 76 R L GROTBECK

UNCLASSIFIED GEP/PH/76-4 NL

1 OF 2
AD
A034006

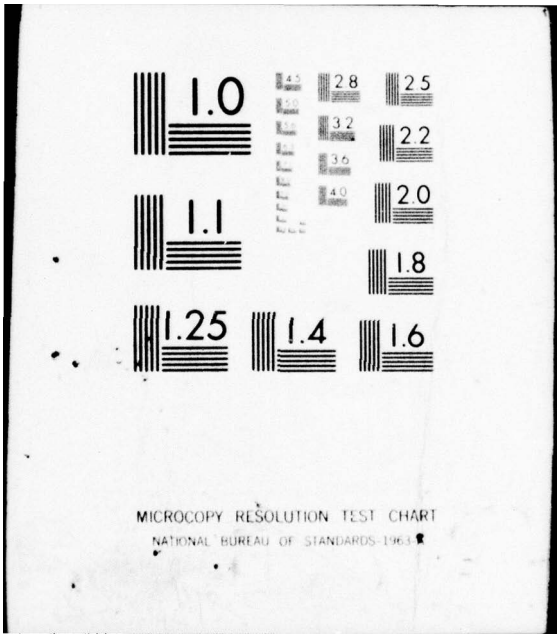
1.0
1.1
1.25
1.4
1.6
1.8
2.0
2.2
2.5
2.8
3.2
3.6
4.0
MICROCOPY RESOLUTION TEST CHART
NATIONAL BUREAU OF STANDARDS-1963-A

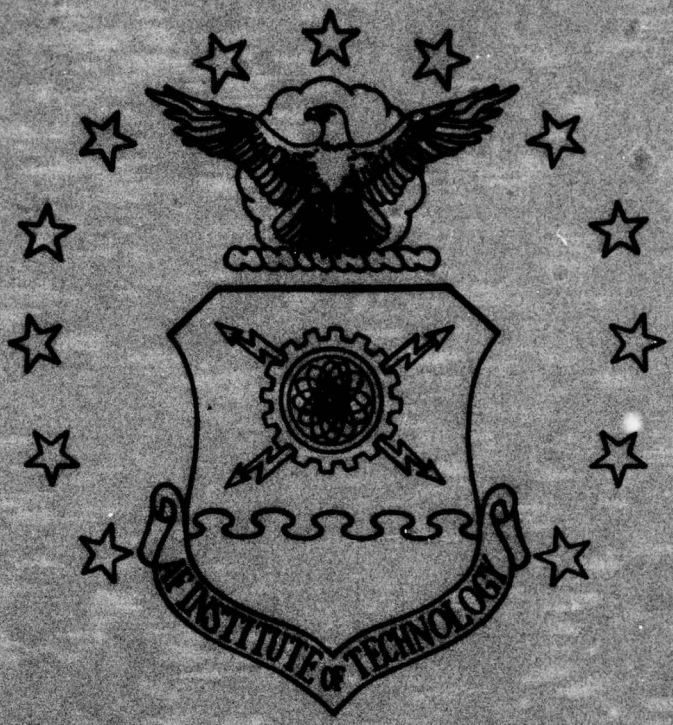

UNITED STATES AIR FORCE

AIR UNIVERSITY

AIR FORCE INSTITUTE OF TECHNOLOGY

Wright-Patterson Air Force Base, Ohio

GEP/PH/76-4

See 1473

AN EXPERIMENTAL INVESTIGATION OF THE RESONANT MODES OF A ROOFTOP LASER

THESIS

GEP/PH/76-4

Ronald L. Grotbeck
Major USAF

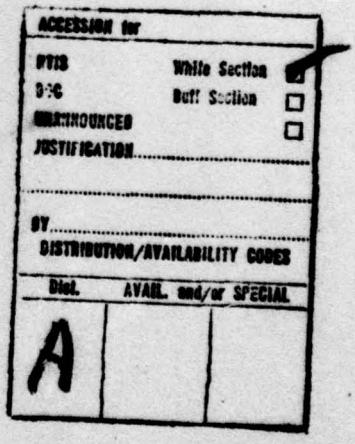

Approved for public release, distribution unlimited.

GEP/PH/76-4

AN EXPERIMENTAL INVESTIGATION OF THE RESONANT MODES OF A ROOFTOP LASER

THESIS

Presented to the Faculty of the School of Engineering
of the Air Force Institute of Technology
Air University
in Partial Fulfillment of the
Requirements for the Degree of
Master of Science
by

Ronald L. Grotbeck
Major USAF
Graduate Engineering Physics
December 1976

Preface

My objectives in investigating the mode structure of roof-reflector lasers was to close the loop, so to speak, on a question which I have put out of my head many times over the past thirteen years: If right-angle roof reflectors really return an incident beam back on itself, why are they not more widely used as laser cavity elements? If I could find a fundamental limitation, something intrinsic to the nature of two-surface reflectors which obviate their use in practical applications, then I could put the question to rest. If not, perhaps I could uncover enough details of their performance to suggest practical design criteria for specific laser systems.

Throughout this study it has been my pleasure to work more intensely and with fewer extraneous distractions than ever before in my scientific career. This is due in large measure to the foresight and competence of the members of the AFIT Physics Department, but more especially to the supportive attention of my family: each one recognised my need for total involvement at critical stages of the research, and each one, in a special way, encouraged my best efforts.

During the period of this research, Captain Howard Evans, a fellow student, has carried out a parallel investigation into the theoretical aspects of roof-resonator operation. His close attention to my experimental work

has been invaluable for avoiding unnecessary measurements, uncorrelatable observations, and blind alleys.

My long-time friend and present thesis advisor, Major Hugo Weichel, enthusiastically supported the project at every stage. His positive encouragement and timely advice sustained my belief in the worth of this research and made the final results more meaningful.

Lastly, special thanks are due to Jan Moore, who carefully deciphered my hasty handwriting to put this manuscript into its present form.

Contents

Contents

Contents

List of Figures

List of Figures

List of Figures

List of Tables

Abstract

A simple roof-reflector theory is developed as a framework for explaining the subsequent experimental observations. The geometrical conditions for obtaining a single "fundamental" spatial mode in a roof-reflector cavity are presented, and the concept of multimode resonance in rooftop cavities is developed. The cavity formed by reflectors with apex angles of 90° is shown to support a large number of simultaneous spatial modes.

First-surface roof reflectors were fabricated with apex angles near 90° and used as resonator elements in a CO_2 laser cavity. Measurements of intensity distribution at the far-field of the resulting outputs were correlated to qualitative observations of near-field intensity so that one might infer optical effects occurring within the resonant structure.

Careful measurements of beat frequencies, present in the laser output beam as high-frequency amplitude modulations and detected with a fast Mercury-Cadmium-Telluride photoconductor, were analyzed to determine the exact composition of spatial modes supported by each of the four cavity geometries studied.

The cavity geometries incorporating 90° roof angles were all found to support many spatial modes. Only the cavity formed by roofs with apex angles less than 90° operated in a single "fundamental" spatial mode.

Peak far-field intensity, output beam divergence, and the sensitivity of both output intensity and output direction to cavity misalignment were measured for each of the four

classes of roof-resonators studied. These parameters were compared with a view toward application of roof-resonator design to practical lasers. Only the crossed-roof configurations were found to have sufficient insensitivity to misalignment in practical applications, and of those, only the <90° geometry was suitable for systems requiring single-mode laser outputs. The 90° crossed-roof resonator provided high output power in a narrow, multimode beam.

Finally, the hypotheses offered to explain the observed operation of the roof-resonators led to suggestions for their optimum utilization in specific applications.

AN EXPERIMENTAL INVESTIGATION OF THE RESONANT MODES OF A ROOFTOP LASER

I. Introduction

Motivation

Laser devices are often used in environments where accelerations and stresses can cause misalignment of the resonator elements. If the output parameters of a particular laser device are at all sensitive to such misalignment, its usefulness for certain applications is severely limited. Military applications are an extreme example of this problem since they usually demand the highest reliability and performance when the environmental conditions are most adverse. Most present-day lasers use resonator elements which are either planar or spherically concave, and are therefore very sensitive to misalignment.

In order to make lasers more useful for applications where stress and vibration cannot be avoided, resonator elements have been fabricated which do not change the angle through which rays are reflected as the reflectors themselves are misaligned. These reflectors are called roof-reflectors because each has two reflecting surfaces which meet at a right angle, resembling a building roof.

Roof-resonator lasers do in fact provide great insensitivity to reflector misalignments, and their use

in operational military applications will begin with the purchase of a rooftop-laser designator (AN/AVQ-25) by the Air Force Avionics Laboratory.

Unfortunately, perhaps, the very feature which makes right-angle roof-reflectors insensitive to misalignment also permits them to support a large number of spatial modes of oscillation in a resonant laser cavity. Since it is possible for each of the spatial modes to have its own propagation direction within the cavity, the output beam of the laser can have a rather large divergence angle. This is certainly undesirable for most applications which generally require a maximum intensity on some far-field target.

The present work is directed towards understanding the mode structure of rooftop-resonators, identifying the parameters which affect the number of modes and their directions of propagation, and if possible, suggesting means to reduce the beam divergence of rooftop lasers.

Methodology

In order to experimentally examine the modes of a rooftop resonator, an electrically-excited carbon-dioxide laser was fitted with various configurations of roof-reflectors and the resulting output beams were measured. In order to simulate the effect of each configuration on the laser intensity at a distant target, the output beams were focused to their far-field plane by a concave mirror. The intensity distribution in that plane was then measured

by translating a sensitive infrared detector across the beam and recording its output. The mode structure was also inferred by measuring the beat frequencies between the several oscillating modes, and by observing the appearance of the near-field and far-field spots on intensity-sensitive imaging plates. Based on these data, the various configurations were compared and general conclusions drawn as to their effectiveness in providing maximum far-field intensity.

Applicability

Throughout this investigation, attempts were made to keep the results generally applicable to the rooftop resonator configurations being studied, rather than specifically applicable to the particular electrical discharge tube used to provide the laser gain medium. To the extent that most lasers have some radial variation of gain and/or refractive index about their axis, the conclusions drawn are valid. For lasers without axial symmetry, or for lasers wherein nonlinear effects change the local propagation conditions within the gain medium, the applicability of the conclusions should be carefully considered. The reflectors used were metallic (gold) external surfaces (ie, the reflectors were not internal reflections within a prism) so concern about entrance window transmissivity or propagation within a material substance should not limit the extension of these 10.6μ results to other wavelengths.

Organization

The remainder of this thesis is organized into seven chapters: a brief theoretical treatment of the properties and operation of rooftop resonators, beginning with a short history of the development of the concept; a description of several preliminary measurements which, though not specifically concerned with the roof-resonator modes, were of sufficient significance to the validity of the final results that they could not be relegated to the appendices; a summary of the experimental procedures employed to measure the resonator output parameters, and some examples of the raw data produced by each measurement; three chapters describing the observed operation of the three rooftop configurations studied (90° rooftop with flat, two 90° rooftops, two $<90^{\circ}$ rooftops); finally, a concluding chapter which compares the operation of the rooftop configuration and outlines some of the criteria for their use. The thesis is followed by a bibliography of technical literature cited and four appendices containing information significant for repeating or extending the present work.

II. Theory

Background

Rooftop reflectors were first suggested as elements of a laser resonant cavity in an unpublished 1958 proposal to ARPA by Gould, who later described the concept of an alignment-insensitive resonator using crossed-roof reflectors (Ref 13:533). Experimental measurements were made in the Netherlands in 1963 by De Lang and Bouwhuis who examined the output of a laser cavity consisting of a $<90^{\circ}$ roof with a flat. They observed a variety of far-field spot patterns and explained them in terms of phase-repetitive travelling waves. (Ref 6:48) Bobroff performed the first theoretical analysis of the modes of a rooftop resonator, but his treatment considered only longitudinal modes of 90° reflectors. (Ref 1:1485). He showed that two eigenpolarizations exist for standing waves in a two-roof cavity, and established the conditions under which travelling waves can exist in such a cavity.

During the ten years prior to 1975, virtually all the work on roof resonators was performed by Italian researchers at the Instituto di Ricerca sulla Onde Elettromagnetiche del Consiglio Nazionale delle Ricerche (CNR). Although their research treated roofs of all angles (from near zero to near flat) and most models were constructed for microwave frequencies, the numerical and experimental results provide significant insights into the operation of near 90° roof-

top resonators at infrared and visible wavelengths. Directly relating to the present work were experiments conducted by Soncini and Svelto, who produced pure transverse modes from a medium quality pulsed ruby rod using rooftop resonators whose roof angles were slightly less than 90°. (Ref 26:261, 27:422). Although only the case of parallel roofs was reported, pure modes were observed for several cavity lengths and roof angles. Ronchi showed analytically that modes of a $<90^{\circ}$ roof resonator have an exponentially low intensity near the edges of the reflectors, so that diffraction at the edges can be neglected. (Ref 22:93). Further analytical work by Pasqualetti and Ronchi provided an integral equation for the eigenfunctions of a resonator formed by parallel roofs of equal angle, which was solved numerically for several real (microwave) sets of resonator parameters. (Ref 19:289 and Ref 20:649).

Checcacci, Falciai and Scheggi analyzed the modes and losses of a 90° roof resonator and their behaviour as the roof edges were allowed to take a finite size. They showed that the roof resonator became equivalent to a rectangular ring resonator as the roof edge dimensions becomes larger than a few wavelengths. During this transition, the zeroth mode of the roof resonator degenerates into its first odd mode ($m = 1$) which is identical to the lowest order mode of the ring resonator. These results were checked by microwave experiments.

(Ref 3:1611). These three researchers then extended their work by considering the case of two counter-rotating sets of modes in the roof-limit of a four-mirror ring resonator. They found that two roof reflectors become essentially a ring-resonator when the roof-edge discontinuity exceeds about six wavelengths. They were also able to verify an equivalence between a 90° roof and Fabry-Perot resonators (in terms of power loss and phase shift versus Fresnel number for the fundamental and first odd modes). (Ref 24:1050).

More recently, Chun and Teppo have analyzed the operational characteristics of an alignment-insensitive Q-switched laser employing two crossed-roof Porro prisms as resonator elements (Ref 5:1942).

Evans is currently performing a detailed theoretical analysis of rooftop cavities from a geometrical standpoint; much of the present experimental investigation has been influenced by his developing understanding of the allowed ray paths in these resonators (Ref 10).

Properties of a Two-Bounce Reflector

When a light ray is incident on a reflecting surface, its angle of incidence is equal to its angle of reflection. Thus, if the angle of incidence is called φ, the angle between the incident ray and the reflected ray is 2φ (Fig 1). If such a reflector is rotated through an angle $\delta\varphi$ so that the new angle of incidence is $\varphi + \delta\varphi$, the angle between the incident and reflected rays is changed by $2\delta\varphi$.

This reflector, when used in a laser resonant cavity, is extremely sensitive to misalignment because oscillator stability requires that rays remain within the cavity after many passes back and forth between the reflectors.

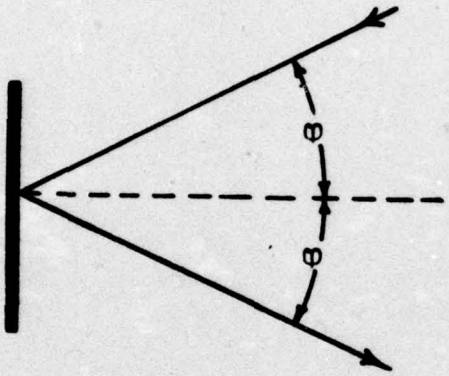

Fig. 1. Reflection from single surface

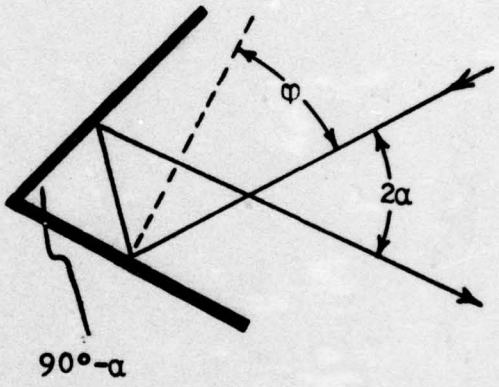

Fig. 2. Reflection from two surfaces

If a reflector is made of two surfaces rigidly arranged so that an incident ray must make an even number of reflections before exiting the reflector, (eg, a rooftop reflector) then the angle between the indident and reflected rays is independent of any rotation, $\delta\varphi$, of the entire reflector about an axis normal to the plane of incidence (Ref 23:1192). Furthermore, as depicted in Fig 2, if the angle between the two surfaces differs from a right angle by an amount, α, then the angle between the incident and reflected rays is just 2α. (Ref 11). The advantages of such a reflector for a laser resonator

are obvious, since misalignments of the reflector cannot change the propagation directions of the field in the cavity.

The Fundamental Mode

In order to realize the full advantage of the alignment insensitivity of two-bounce reflectors, it is necessary to install them in the laser cavity with their roof-edges crossed. In this way, misalignment of one of the reflectors about an axis in its plane of incidence (tipping its roof edge) is equivalent to a rotation of the opposite reflector about its roof axis. The net result of such a maneuver is to translate the optical axis of the resonator, which is along the line perpendicular to both roof edges. In this regard (translating the optic axis), a roof resonator is not completely insensitive to misalignment since any real resonator has some finite aperture (faces of a solid gain medium, electrodes for producing a discharge in a gaseous gain medium, windows, etc.); if a misalignment is severe enough to translate the axis to the edge of one of the apertures of the system, some effect on the laser output will occur. This is not a fundamental limitation of the resonator, however, since (in principle) apertures may be made as large as required for any particular application.

Fundamental to the roof resonator is the path or pattern which the rays trace between the reflectors. The pattern depends intimately on the roof angle of the reflection and the geometry of the cavity. Clearly, if

the roof angle is so small that a ray from one roof is not returned to that roof after reflection, then the closed path required for laser oscillation cannot occur. This is also a case of an aperture being too small or too distant, as depicted in Fig 3:

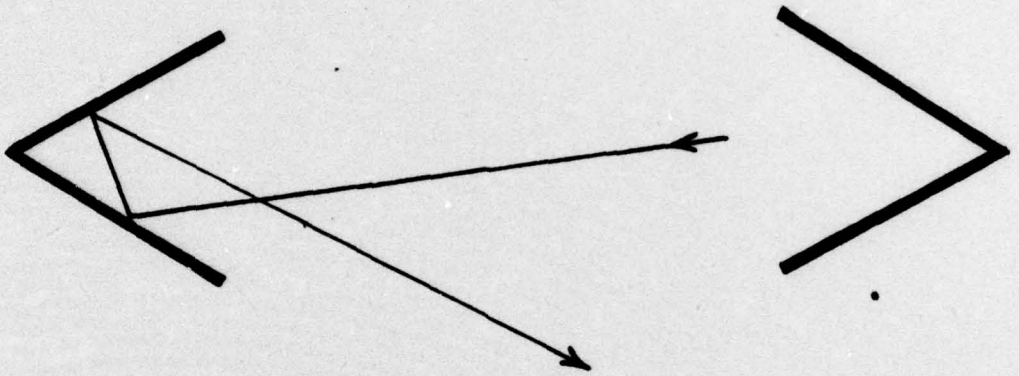

Fig. 3. Unstable condition

Actually the unstable condition occurs when any aperture in the system prevents a ray from returning to its point of origin. The problem of stability then is essentially a geometrical one: determine whether the limiting apertures of a system are large enough to allow a ray to resonate along a closed path between the reflectors.

Fig 4 shows the path of a ray which just misses the aperture edges to close upon itself. All rays not coincident with the one drawn are intercepted by one or the other of the apertures and do not form closed paths. Fig 4 represents an idealized case for which both roof angles are identical. In a real resonator, the unavoidable differences in the roof angles make an exact closed path impossible if

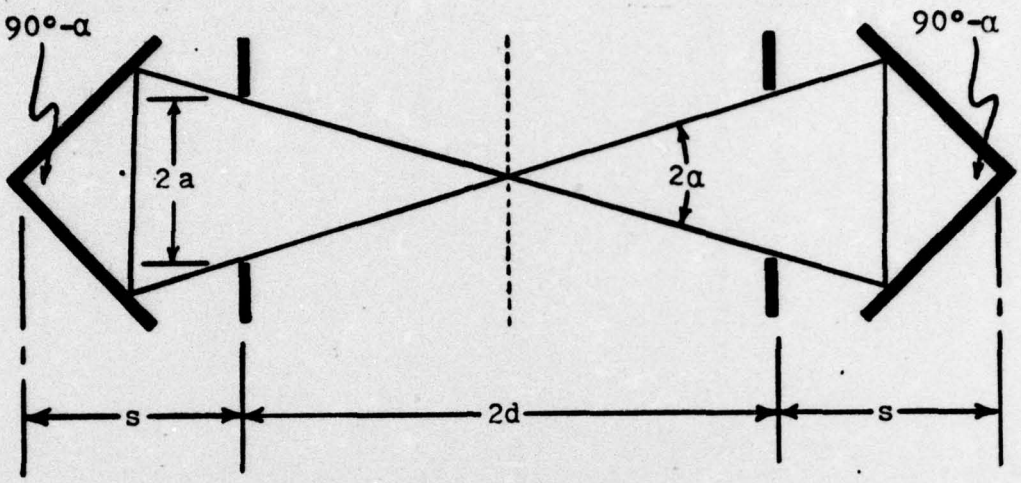

Fig. 4. Stable condition (limit)

the roof edges are parallel (i.e. a ray "walks off" the idealized path and intercepts the aperture edge after a few round trips).

The situation is different for the case of "crossed" roof edges. The actual three-dimensional ray path between crossed roof reflectors cannot be truly represented by the two-dimensional drawing in Fig 4, which is only a projection of the ray path onto a plane orthogonal to the roof edges. However, the projected ray path depicted in Fig 4 for parallel-roof reflectors is identical to the <u>projection</u> of the ray path between crossed roofs, if one of the roof edges lies along the dashed line which divides the figure. In that case, the projected angle of incidence on the (crossed) reflector is equal to the projected angle of reflection. Thus, <u>in the projection</u>, one of the reflectors acts like a plane mirror. The projected ray path, reflector, and aperture on the right side of Fig 4 can therefore be

considered as the virtual images of the projected ray path, reflector, and aperture on the left (reflected through the dashed line representing the crossed roof edge). The projected ray path in this case depends only on the roof angle of the left reflector.

The ray paths between crossed roofs are always closed (exactly), even if the roof angles are not identical. The only requirement for stability in a crossed-roof resonator is that the apertures be large enough to permit the path to close. Geometrical examination provides the relation between aperture size and roof angle for crossed roofs a distance L = s+d apart:

$$90° - \alpha = 90° - \tan^{-1} \frac{a}{d} \qquad (1)$$

The amount by which the roof angle differs from a right angle is a convenient parameter for characterizing roof reflectors. The maximum value of this "roof-angle" parameter for a stable resonator is

$$\alpha_m = \tan^{-1} \frac{a}{d} \qquad (2)$$

For reflectors with this roof angle, the ray path consists of the single ray drawn in Fig 4. This condition therefore utilizes the very minimum mode volume of whatever gain medium exists in the space between the reflectors, and is truly a limiting case of this type of resonator.

The Corner Limit

If roof angles of $\alpha < \alpha_m$ are allowed, then a number of other rays can exist parallel to the "limiting ray" of Fig 4. This case is depicted in Fig 5, which is a projection of the

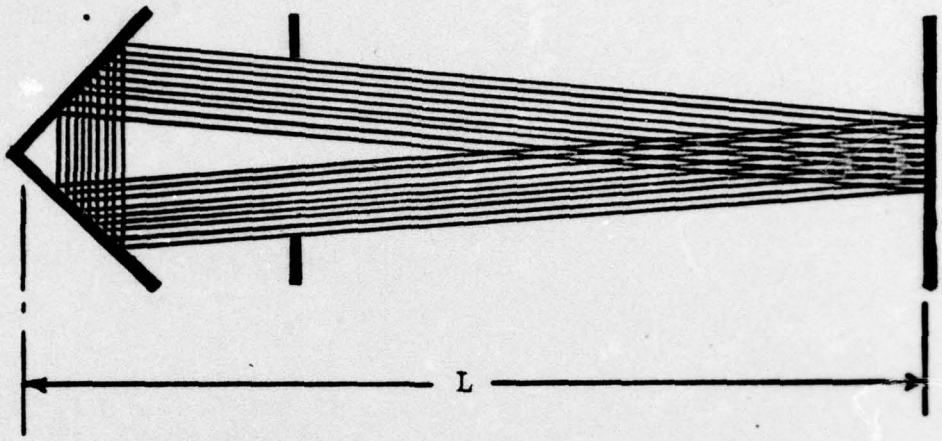

Fig 5. Fundamental Mode

ray bundle between "crossed" roof reflectors. The roof edge of the right reflector is projected as a solid line segment and, in the projection, acts as a plane mirror. From Fig 5, one can see that a ray near the edge of the bundle must make two circuits (four one-way passes) between the reflectors before closing on itself. One might expect an axial mode spacing of $\frac{c}{4L}$ when the phase-repetitive condition for stimulated emission is satisfied. Notice, however, that all the rays travel the same distance in a <u>single</u> round trip from the right reflector to the left and back. All the rays therefore maintain a constant phase relationship across the "width" of the ray bundle. Thus the phase-repetitive condition holds for all the rays of the bundle after only one circuit, producing an axial mode spacing of $\frac{c}{2L}$. This also explains the seemingly anomolous measurement of "axial"

mode separation (of $\frac{c}{2L}$) by De Lang and Bouwhuis, who expected a value of $\frac{c}{8L}$ for their three-mirror resonator (Ref 6:50).

The fundamental mode exists for all values of roof-angles between α_m and the angle which produces the pattern depicted in Fig 6:

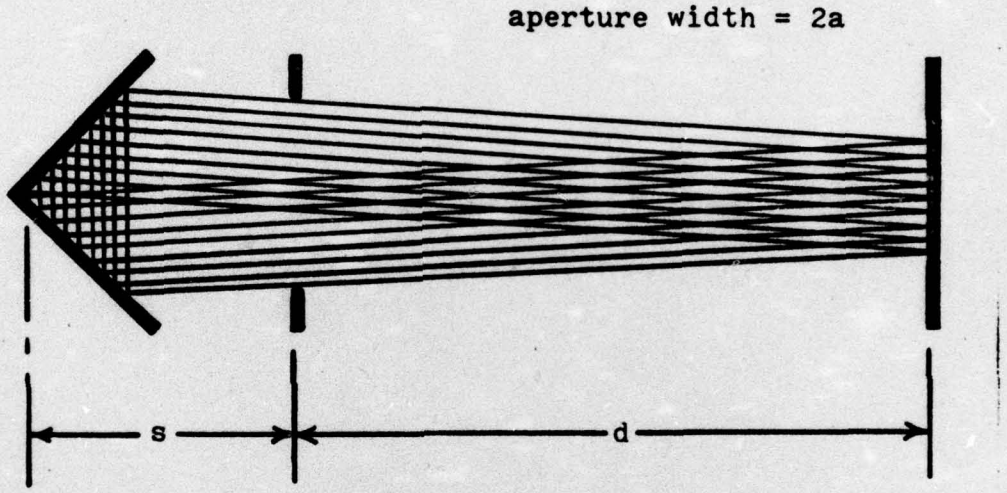

Fig 6. The Corner Limit

In this pattern, the roof edge (corner) of the reflector is the limiting aperture of the ray bundle. This unique case is therefore called the "corner limit". The roof angle at which the corner limit is reached is

$$\alpha_1 = \tan^{-1} \frac{a}{s+2d} \approx \frac{a}{s+2d} \qquad (3)$$

for small α.

Since this pattern of rays makes use of the maximum mode volume in the available gain medium, it is a true limiting case for the fundamental mode. In practice, one

would want to operate as close as possible to this corner limit while maintaining the fundamental mode condition: $\alpha_1 < \alpha < \alpha_m$. Three practical considerations are worth noting about the fundamental mode.

First, the reflector drawn as a single vertical line in Figs 5 and 6 is really a roof reflector with its own roof angle (which is, in general, not equal to the angle of the roof reflector at the left sides of the figures; in practice it is impossible to make both roofs exactly equal). Thus the real, three-dimensional ray bundle resonating between two crossed roof-reflectors may not have a symmetric cross-section. In addition, travelling waves can propagate along the ray paths of Figs 5 and 6 in either of two directions. Since the three-dimensional ray bundle then has two distinct propagation directions in the (projected) plane of the figures, and two more propagation directions projected into a plane orthogonal to the figures, there are in fact four separate propagation directions within such a cavity. Under certain output coupling conditions, four separate output beams are possible from a crossed roof-reflector.

Secondly, misalignment of either reflector about its roof axis has no effect on the ray patterns, whereas misalignment about an axis parallel to the opposite roof deforms the ray bundle as depicted in Fig 7:

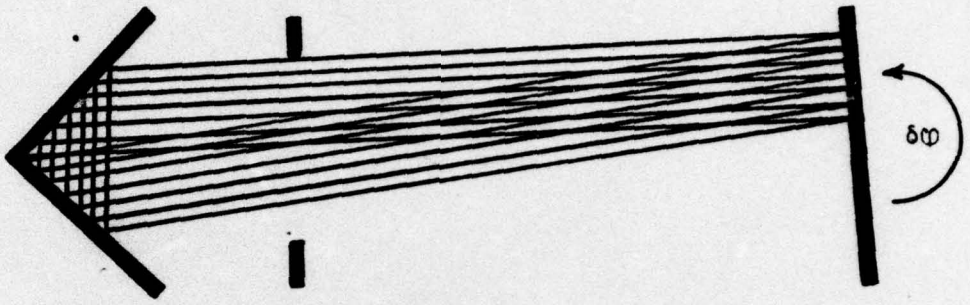

Fig. 7. Misaligned crossed-roofs

This deformation is really just a reduction of the mode volume occupied by the bundle, since the lower edge of the aperture is no longer the limit for the edge ray. The effect, however, is a reduction in overall output power of the laser device (though certainly not as severe a reduction as a similar misalignment of plane mirrors would cause for an equivalent mode volume).

Thirdly, the reflecting surface near the roof-edge does not contribute to the cavity oscillation until α has decreased to near the corner limit. Thus imperfections at the edge of roof reflectors pose no serious operational drawback for $\alpha_1 < \alpha$.

Higher-order Modes

If the roof angles of the reflectors are increased

beyond the corner limit (ie, $\alpha < \alpha_1$) then the path of rays in the cavity becomes as depicted in Fig 8:

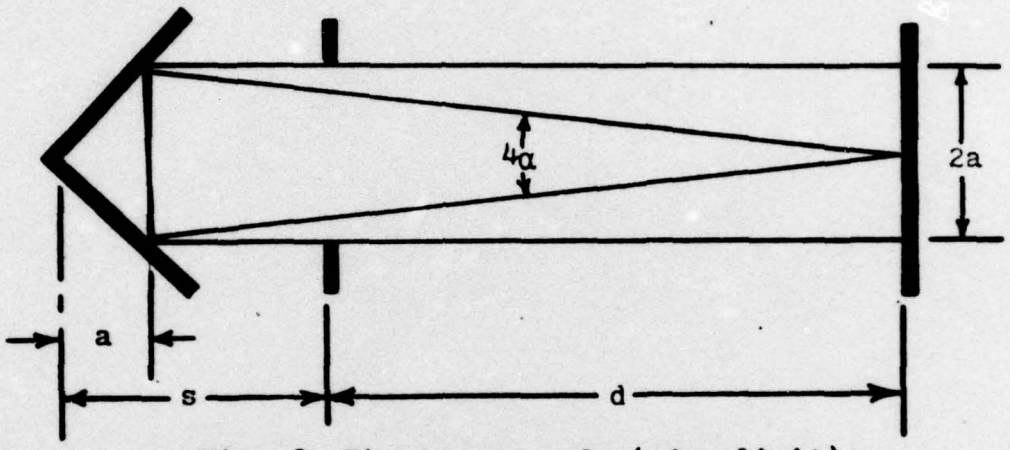

Fig. 8. First even mode (edge limit)

By inspection of the figure,

$$\alpha_e = \tfrac{1}{2}\tan^{-1}\frac{a}{d+s-a} \approx \frac{a}{2d+2(s-a)} \qquad (4)$$

for small α.

Comparing this with equation (3), we see that this pattern exists for roof angles only slightly larger (α slightly smaller) than the corner limit, since 2(s-a) is generally small compared to d. The ray drawn in Fig 8 is an edge limit of this mode and so occupies a minimum mode volume (ie, its ray bundle consists of a single ray). At this roof angle, the fundamental mode pattern is still supported by the cavity, but at reduced mode volume.

As the roof angle is increased, the mode volume of the fundamental mode continues to shrink and that of the first even mode (m = 2) increases. A limit is again reached when

the mode volume of the first even mode is a maximum, as depicted by Fig 9:

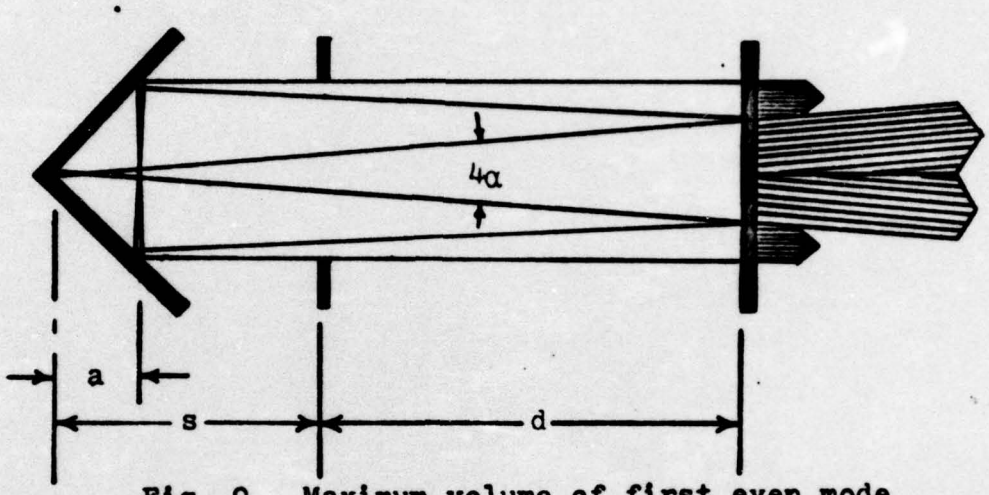

Fig. 9. Maximum volume of first even mode

Since cross-hatching the ray bundles would hopelessly cover the edge-rays drawn in Fig 9, the possible output beams are shown emerging from the right reflector. They provide some indication of the direction and dimensions of the ray bundles of the first even mode. The roof angle at this limit is

$$\alpha_2 = \tfrac{1}{2}\tan^{-1}\frac{a}{2s+2d-a} \approx \frac{a}{4d+2(2s-a)} \qquad (5)$$

Table I
Roof Resonator Mode Parameters

Mode Number	Number of Propagation Directions	Angles Between Output and Axis
1	2	α
2	3	0, 2α
3	4	α, 3α
4	5	0, 2α, 4α
5	6	α, 3α, 5α

The 90° Roof Reflector

As the roof angle continues to increase beyond α_2, the mode volume of the first even mode (m = 2) begins to decrease because its ray bundle becomes limited by the aperture; the mode volume of the fundamental mode, already small at α_2, is reduced still further; and modes of even higher order appear. The crucial point is that the lower order modes do not disappear when the cavity parameters permit modes of higher order - they simply occupy a smaller mode volume. Each of the modes has its own output direction and characteristic divergence, and a multimode beam will contain components of all of them.

Therefore, when the roof angle has increased to exactly 90° we expect the pattern depicted in Fig 10:

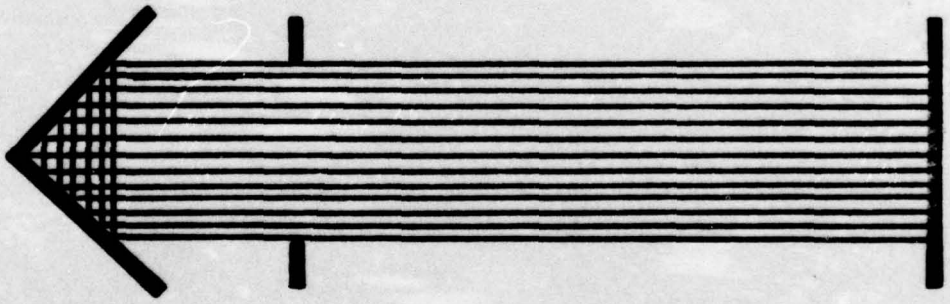

Fig. 10. Crossed 90° roof resonators: the n^{th} mode

In this case, each mode occupies an infinitesimally small volume, with the lower order modes nearer the center of

the resonator. Since every even mode has one of its propagation directions along the resonator axis, a substantial amount of power will be contributed in that direction by the collection of modes, however small their individual mode volumes. The problem is that there may also be substantial amounts of power in other directions.

Interpreting the 90° roof resonator as a structure which supports a large number of modes provides a very realistic model of actual laser devices. The models which treat the axially directed rays as an inherently stable "zeroth-mode" neglect the effects of small roof-angle errors, refractive index variations along the gain path, and diffraction by aperture and roof edges. Zeroth-mode models assume that energy reflected, refracted, or diffracted into small off-axis angles by those effects does not find a phase-repetitive closed path within the structure and so does not play a significant role in eventual energy extraction. The $n^{\underline{th}}$ mode limit model, on the other hand, provides a large number of closed-path alternatives for rays travelling at small angles to the axis; it predicts the existence of many modes, with slightly different propagation directions, in real 90° roof resonators.

III. Preliminary Measurements

Small Signal Gain Measurements

Motivation. Before the investigation of rooftop resonator modes could begin in earnest, several preliminary measurements were necessary to establish the optimum configuration of the laser gain medium and the output coupler. The first of these, the small signal gain, was performed in an attempt to make the CO_2 discharge volume as homogeneous as possible. The specific intention was to avoid an excessive current density along the longitudinal axis of the plasma which would overheat the plasma. Normally, energy dissipated in the plasma column is diffused to the walls of the discharge tube with sufficient rapidity so that the center of the column is not much hotter than the edges (although there is always some radial temperature gradient). If the energy is dissipated faster than it can be carried to the walls, the temperature at the center becomes high enough to reduce the optical gain along the axis. When this occurs, the gain medium becomes annular in shape and any investigation of spatial mode structure is highly dependent on that particular gain profile.

Methodology. Since the gain medium could not be made completely homogeneous in this large-bore longitudinal discharge, (see Appendix A) the gain was optimized for the center of the plasma column. In this way, any transverse

variation of gain has at most a quadratic dependence on radial position. The resulting influence on the mode structure of the roof resonator at least approximates that induced by the gain media of most solid-state laser systems and all properly operated gaseous-discharge systems.

There is a conspicuous lack of unanimity among the investigators of CO_2 discharge lasers as to the optimum mixture of the constituent gases. (Ref 17:275, Ref 7:155, Ref 21:21, Ref 4:170). Cheo's chapter on CO_2 lasers is the most complete; information contained therein indicates that a product of CO_2 partial pressure and tube diameter of 3 torr-cm is optimum for a flowing system (Ref 4:173), which implies an optimum CO_2 partial pressure for the 1.5 cm discharge tube of 2 torr. The same reference indicates that gain increases in flowing systems as Helium pressure is increased to 3 torr, and is relatively insensitive to further increases in the partial pressure. Cheo's figure 21 (Ref 4:175) shows a gain of 500%/meter for a 12 mm bore tube with partial pressure ratios of CO_2: N_2: He:: 2: 1.5: 4 (slow flowing system).

Considering the above recommendations, nominal nitrogen and helium partial pressures of 1.5 torr and 4.0 torr respectively were maintained while the optimum carbon dioxide pressure was determined. Then that optimum CO_2 pressure was maintained (with 4.0 torr of He) while the optimum N_2 pressure was determined. Finally, the insensitivity of gain to He pressure above 3 torr was checked.

The gain was optimized by directing the unpolorized output beams of a Coherent Radiation Laboratories (CRL) model 42 CO_2 laser down the center of the operating plasma column (with resonator elements removed) and measuring the power of the beam after amplification by the gain medium (power was measured using a Quantronix power meter). The plasma discharge was then turned off and the transmitted power (unamplified) again measured. The ratio of hot-cavity-output to cold-cavity-output then provided a measure of the relative gain of the medium (not true single-pass gain since input power was not measured at this time and losses were as yet unknown. Single pass gain calculations are made in the last part of this section).

These relative gain measurements were taken for a range of discharge currents at a specific combination of partial pressures of the constituent gases required for CO_2 laser operation. By repeating this gain-versus-current measurement for a large number of different combinations of the gas partial pressure, the optimum partial pressure of each gas was determined (and also the optimum current).

The CRL probe laser was then configured for polarized output (oriented for maximum transmission through the Brewster windows of the discharge tube) and the input and output power of the beam measured at the optimum combination of gas partial pressures and current. With this data, true small-signal-gain for a polarized beam was determined.

Variation of Carbon Dioxide Partial Pressure. With nitrogen and helium partial pressure maintained at 1.5 torr and 4.0 torr respectively, relative gain-versus-current data were taken for values of carbon dioxide partial pressures from 1.0 torr to 3.5 torr in 0.5 torr increments. A typical set of these data for 2.0 torr CO_2 are plotted in Fig 11:

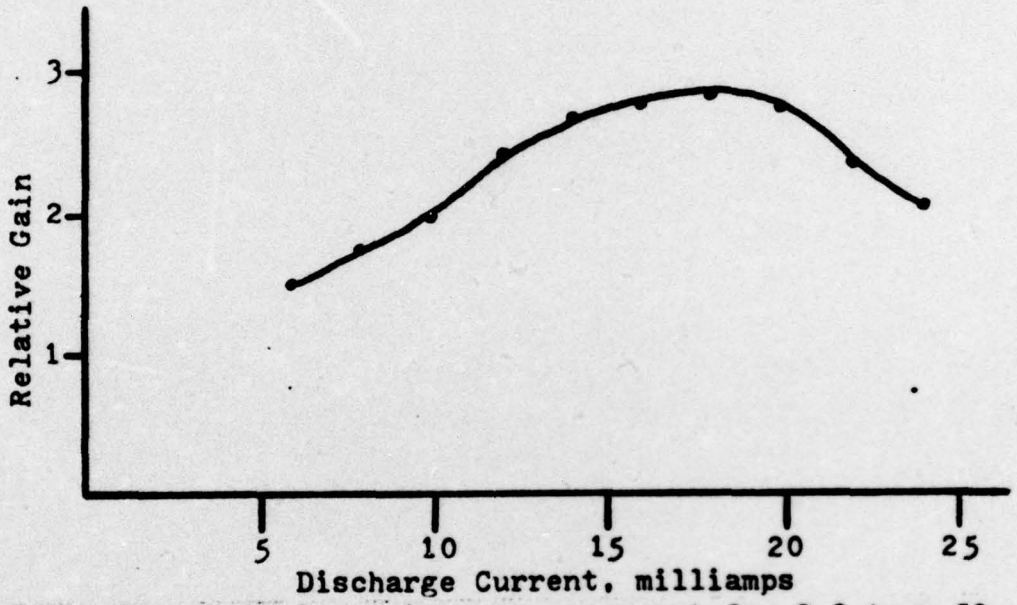

Fig. 11. Relative gain versus current for 2.0 torr CO_2

The several sets of data for the different CO_2 pressures had peak gains at slightly different values of current between 16 and 22 milliamps. The average value of the optimum current is 18.4 ma, but the gain-versus-current variation is not sharply peaked for any of the CO_2 concentrations; 18 ma was therefore used as an acceptable compromise. The relative gain measured at 18 ma for each CO_2 concentration is shown in Fig 12:

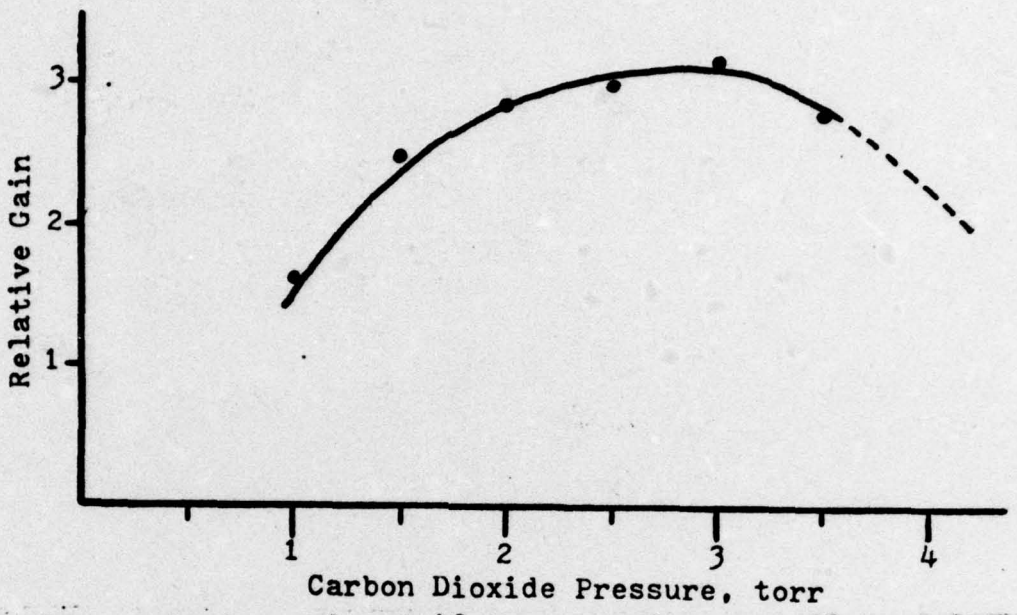

Fig. 12. Relative gain at 18 ma current versus CO_2 pressure

From these data, 3.0 torr partial pressure of CO_2 was chosen as optimum; a current of 18 milliamps was chosen as providing the largest relative gain.

Variation of Nitrogen Partial Pressure. With carbon dioxide partial pressure set at its newly-determined optimum value, the helium pressure maintained at 4.0 torr, and discharge current kept at a constant 18 milliamps, nitrogen partial pressure was varied from 1.0 torr to 4.0 torr in 0.5 torr increments. Fig 13 shows the variation of the relative gain observed under these conditions:

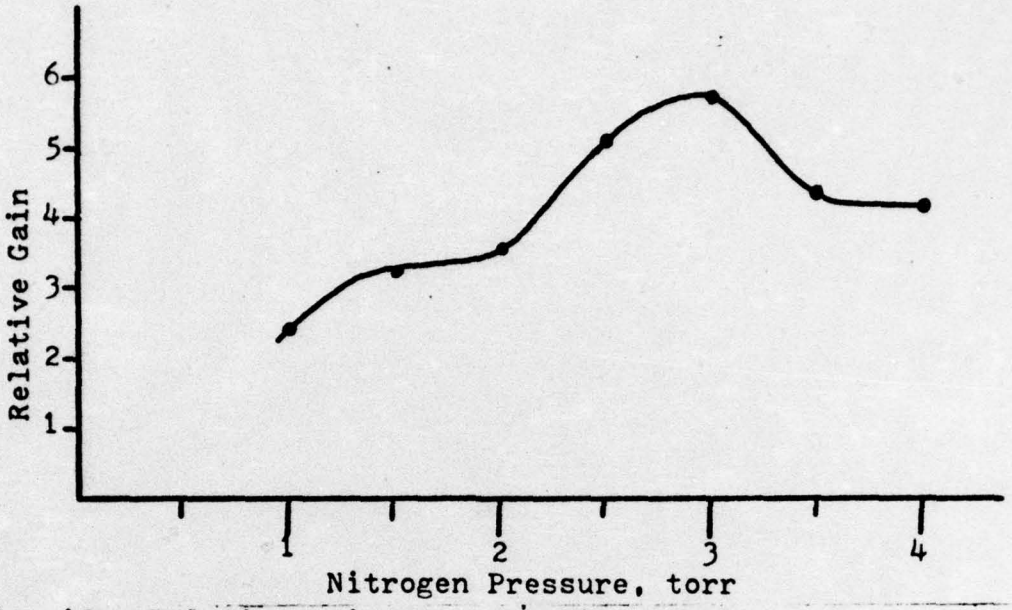

Fig. 13. Relative gain as a function of nitrogen pressure

From these data 3.0 torr partial pressure of nitrogen is chosen as optimum.

Variation of Helium Partial Pressure. With carbon dioxide and nitrogen partial pressures both maintained at 3.0 torr, and current constant at 18 ma, the partial pressure of helium was increased from its nominal value of 4.0 torr. Fig 14 summarizes the resulting gain variation. Though not conclusive, the helium data does not disagree with Cheo's assertion that increasing He pressure above 3 torr does not significantly enhance gain (Ref 4:171). Since a He pressure of 4.0 torr was sufficient to provide near-maximum gain, and since 10 torr total pressure insures that the 00°1 - 10°0 vibrational transition of CO_2 will be homogeneously broadened by collisional processes (at least broadened enough that only a single axial mode can exist

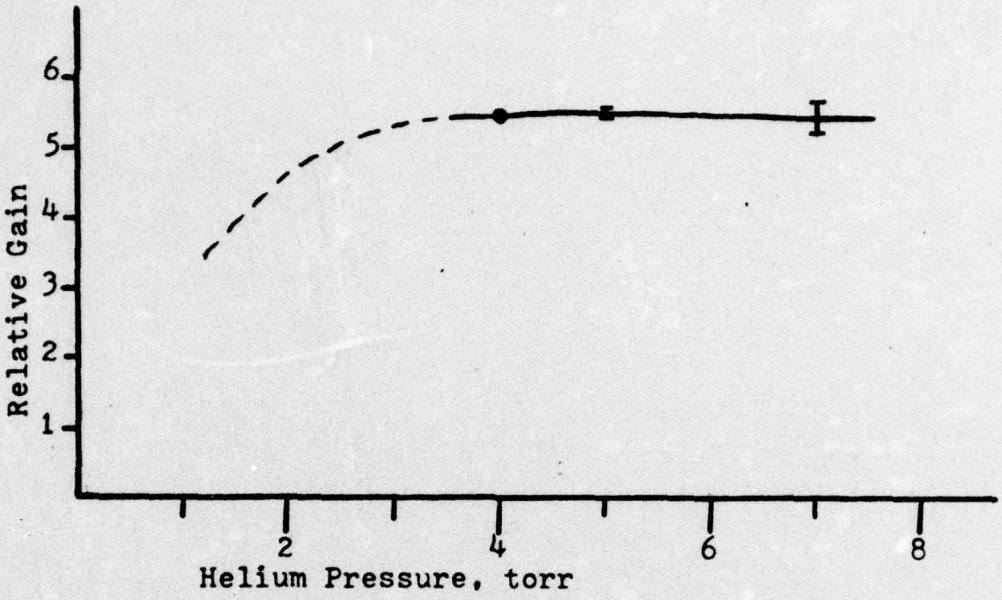

Fig. 14. Relative gain variation with helium pressure

within the approximately 100 MHz wide gain profile) (Ref 12:227), He pressure of 4.0 torr was chosen.

The standard operating configuration for the laser gain medium during the remainder of this study was therefore established:

3.0 torr CO_2 pressure
3.0 torr N_2 pressure
4.0 torr He pressure
18 ma discharge current

Single Pass Gain and Loss. To complete the determination of the small signal gain for the laser gain medium under the above "standard conditions", the absolute single-pass gain of the discharge (taking losses into account) was measured. To match the loss conditions which would exist when the discharge tube and its Brewster-angle salt windows were part of an oscillating cavity, the CRL probe laser was

configured for polarized output, oriented for maximum transmission through the discharge tube windows.

To complete the losses which the probe beam experienced in passing through the gain medium (consult Appendix A for details and dimensions of the discharge tube), the probe beam was determined to have an approximate gaussian intensity profile with a waist of 2.5 mm at its output from the CRL laser. Siegman (Ref 25:308) gives the beam spot size at any distance, z, from the waist as

$$w(z) = w_o \sqrt{1+\left[\frac{\lambda z}{\pi w_o^2}\right]^2} \qquad (6)$$

where w_o is the waist and λ is the wavelength.
Since the probe laser entered the CO_2 discharge tube 3.54 meters from the CRL laser output, its spots size at that point was w_{in} = 5.39 mm. The probe laser was apertured by the 11 mm diameter electrode (4.23 meters from the waist) before it exited the discharge tube, and by equation (6) its spot size there was $w_{aperture}$ = 6.23 mm.

Siegman also gives the fraction of a gaussian beam passing through an aperture (Ref 25: 312):

$$\frac{Ia}{I_o} = 1-\exp\left[\frac{-2a^2}{w^2}\right] \qquad (7)$$

where a is the aperture radius.
At the electrode, a = 5.5 mm so the fraction of the beam exiting the discharge tube a was $\frac{Ia}{I_o}$ = 0.790. The actual powers transmitted through the exit window of the tube was 380 milliwatts with no discharge (the power meter has an

aperture of 16 mm diameter, so all the power passing through the 11 mm electrode aperture was collected). The input power was also measured (with the 16 mm diameter aperture) at 475 milliwatts, but using equation (7) this was only 0.987 of the total beam power at the input. The output power measurement implies a total beam power of $\frac{380}{.790} = 481$ milliwatts, whereas the input power measurement implies $\frac{475}{.987} = 481$ mw for total beam power. This remarkable agreement indicates that window losses (scattering, absorption, vignetting) are practically negligible (as is absorption by the "cold" gain medium at standard conditions).

The input and output power was measured in the same manner as above while the 18 ma current was being discharged through the plasma (hot cavity). The values measured were $P_{in} = 425$ mw, $P_{out} = 1350$ mw. Correcting for the previously determined aperture transmission fractions, the true single-pass gain of the cavity is

$$G = \frac{1350}{425}\left[\frac{.987}{.790}\right] = 3.97 \qquad (8)$$

Output Coupler Selection

Determination of Required Feedback. From the results of the small-signal gain measurement, a computation of the optimum output coupling was made for the CO_2 gain medium under "standard conditions". Weichel and Pedrotti give the optimum mirror transmission as (Ref 30:26):

$$T(opt) = L\left[(\alpha\gamma)^{\frac{1}{2}} - \alpha\right] \qquad (9)$$

where L is the length of the medium, α is the absorption

per unit length, and γ is the gain per unit length. In terms of the single pass power gain and loss these are

$$\gamma = \frac{G}{L} \quad , \quad \alpha = \frac{A}{L} \tag{10}$$

where G is defined by equation γ and A is the single-pass attenuation.

Equation (9) can be rewritten in terms of these single-pass quantities

$$T(opt) = (AG)^{\frac{1}{2}} - A \tag{11}$$

The quantity A can be determined from a consideration of the diffraction losses (since we have seen that attenuation by the windows and cold medium are negligible).

For a nominal cavity spacing of L = 2 meters and a limiting aperture (inside radius of the electrodes) of a = 5.5 mm, the cavity Fresnel number (for the 10.6μ CO_2 wavelength) is:

$$N = \frac{a^2}{L\lambda} = 1.427 \tag{12}$$

For this Fresnel number, Heard gives the diffraction loss per pass to be A = 0.12 (Ref 14:271). The optimum transmission of the output coupling reflector is then

$$T(opt) = \sqrt{.12 \times 3.97} - .12 = 0.57 \tag{13}$$

Echbreth has shown that the coupling fraction for lasers with a low gain-length product ($\gamma L < 5$) must be substantially lower for a travelling-wave oscillation than for a standing-wave (Ref 9:797).

Analysis of his figures 4 and 5 (which were generated for a single-pass cavity loss of 0.17) indicate that at a

single-pass gain G = 4, the travelling wave output transmission should be 70% of the value calculated as optimum for the standing wave. Since Babroff has shown (Ref 1:1487) that a cavity formed by two crossed rooftops supports both standing waves and travelling waves, it would seem that the choice of output coupling for a roof resonator is a dilemma. Closer analysis of Eckbreth's development reveals, however, that the travelling-wave for which he calculates optimum output coupling is that which exists in a ring-resonator making only one pass through the gain medium per reflection on the output coupler. While the roof-reflector certainly behaves like a ring resonator (Ref 3: 1611 and Ref 24:1050), the type of output coupling arrangement used determines whether a travelling-wave interacts once or twice with the output coupler during a single round trip (two passes) through the gain medium.

If coupling is achieved by inserting a partially reflecting plate into the cavity as a beamsplitter, each wave travelling around the ring makes two output reflections per round trip. If coupling is achieved by making one surface of one of the roofs partially transmitting, then each travelling wave in the cavity makes only one output reflection per round trip. Applying Eckbreth's conclusion to equation (13), the reflectivity of the output coupler must either be

$$R_1 = 1-T_{opt} = 0.43 \qquad \text{(for one output reflection)} \quad (14)$$

$$R_2 = .7\ T_{opt} = 0.40 \qquad \text{(for two output reflections)} \quad (15)$$

The form of equation (15) occurs because, for the case of the reflector inserted into the cavity, the output coupling fraction is the reflectivity of the coupler rather than its transmissivity.

Available Coupler Configurations. Several techniques for coupling energy out of a roof resonator have been reported.

De Lang and Bouwhuis used a partially-reflecting flat as one resonator element opposite their roof reflector (Ref 2:48). Soncini and Svelto allowed energy to escape their cavity as an evanescent wave by frustrating the internal reflection of one of their (solid) resonator elements (Ref 26:261 and Ref 27:422). Chun and Teppo took advantage of the birefringence of a calcite prism to refract a beam out of their cavity after rotating its polarization with a linear electro-optic switch (Ref 5:1942). All these techniques provide only one output reflection per round trip of the cavity. The obvious technique of inserting a flat plate into the cavity has not been reported, perhaps because of the disadvantage of having the available power divided between two output beams. In spite of this practical limitation, the single-plate coupler was considered for the rooftop-resonator investigation.

Since the partially-reflecting flat could not be used as a resonator element in a cavity consisting of two roof-reflectors, that output coupling technique was rejected as being too specific to a particular configuration. The

birefringent prism was also rejected as an output coupler since materials from which to fabricate such a prism and its associated electro-optic switch were not available (with good transmission at the 10.6μ wavelength). A technique equivalent to the frustrated reflection from one of the roof surfaces was suggested by Towles (Ref 29). It consisted of replacing one of the totally-reflecting surfaces of one of the roof-reflectors with a partially-transmitting dielectric or semiconductor flat. This arrangement is subsequently called a "Towles coupler".

A limited number of partially-reflecting materials was available, as summarized in table II.

Table II
Available Output Coupling Materials

Material		Index @ 10.6μ	Reflectivity @ 45° // polarized	⊥
ZnSe	20m x 30 x 3	2.41	.079	.281
NaCl	5 x 50 (diam)	1.465	.007	.084
Ge	5 x 50 (diam)	4.0	.234	.484

Initial attempts to use the Zinc Selenide chip were unsuccessful. Inserting the chip into the resonant cavity at any angle caused lasing action to cease altogether Subesequent examination of the chip showed both optical surfaces to be irregularly non-planar, so that the chip acted as a lens whose focal length varied with position. ZnSe was therefore abandoned as a possible output coupler for this study.

Sodium Chloride as an Output Coupler. Even though the reflectivity of the salt flat is too low to be useful in a Towles coupler, an attempt was made to use it to extract useful output at a large angle of incidence (with the cavity radiation polarized perpendicular to the plane of incidence).

A 2-meter resonant cavity was set up and aligned using the gold-coated flat (reflector "F_1") and roof-reflector "C". (See appendix C for desctiption of the reflectors). The roof edge of "C" was horizontal, perpendicular to the polarization of the radiation, and the output coupler was between the roof and the gain medium.

A representative distribution of intensity in the near-field of the output beam was recorded by allowing the radiation to darken a sheet of Thermo-Fax paper (Fig 15).

Fig. 15. Near field of F-C resonator through NaCl flat

There were several patterns produced by this resonator configuration; their far-field intensity distributions were observed by focusing the beam with a spherically concave reflector of 4.5 meters focal length. These far-field patterns were recorded on Thermo-Fax paper. They are reproduced in Figure 16 and are tentatively identified from left to right as TEM_{01}, TEM_{10}, and TEM_{11}.

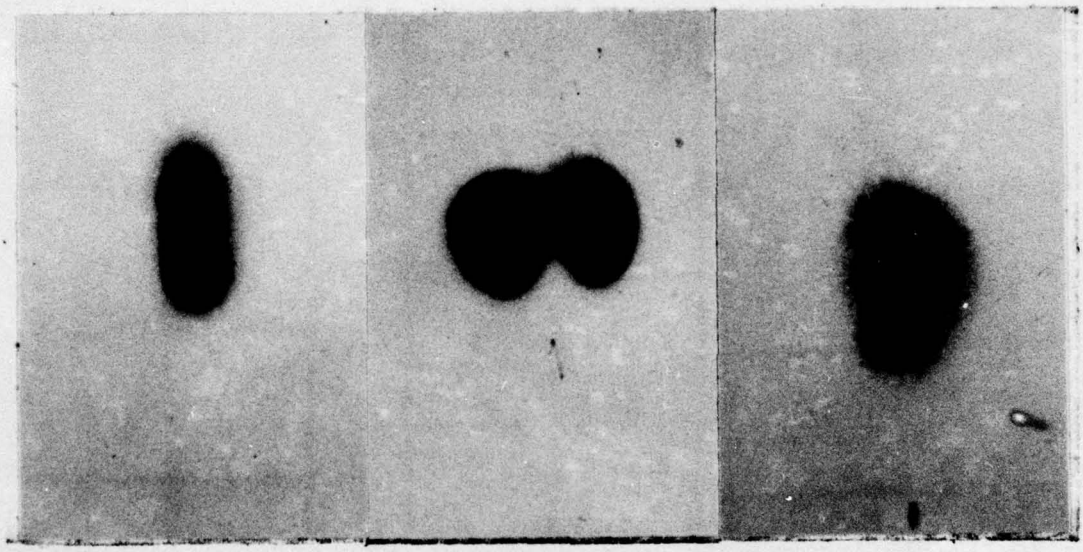

Fig. 16. Far-field intensity patterns of F-C resonator through NaCl flat

These intensity patterns could be changed by adjustment of the cavity-flat alignment; but even though the several patterns appeared to be quite distinctive, there was no identifiable position of the cavity-flat which would reliably reproduce them. In fact, each blended more or less continuously with the others, and the laser moved from one to the other in a spontaneous and random manner if left alone. The pattern in the center of Fig 16 appeared to predominate.

Essentially the same results were obtained when roof-reflector "C" was replaced with another gold coated flat, (Reflector "F_2") indicating that the patterns were not an artifact of the rooftop configurations.

When one of the gold flats was replaced by a partially transmitting germanium flat (Reflector "F_3") and the salt coupler removed from the cavity, the far-field of the beam transmitted through the germanium showed a single intensity lobe (as Fig 17 shows):

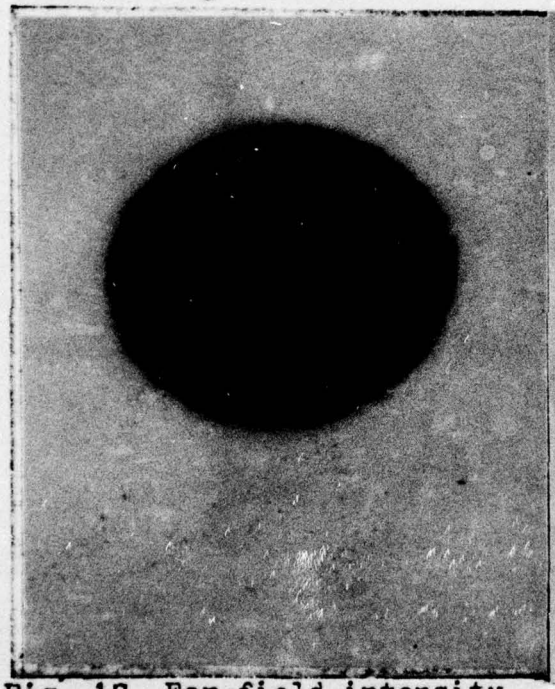

Fig. 17. Far-field intensity pattern of F_1-F_3 resonator through Germanium.

Fig. 18. Far-field intensity patterns of F_1-F_3 resonator with NaCl flat in cavity.

As can be seen in Fig 18, inserting the salt flat into the cavity somehow favors the production of higher-order Hermite-gaussian modes. Figs 17 and 18 are the far-field of the same output (transmitted through the germanium flat) under the same conditions. The only difference was the presence of the salt flat in the cavity (at about 60° angle of incidence).

It was at this time that the reason for the temporal instability of the modes of Fig 16 was determined. Heaters placed near the Na Cl Brewster windows of the discharge tube to reduce their deterioration by atmospheric moisture were creating tiny turbulent cells which bubbled up through the beam path. The resulting variation in the local refractive index was enough to cause the output power to fluctuate along with the beam spot.

Based on the qualitative observations of the influence of the salt flat on the far-field intensity distributions of these resonators, especially the F_1 - F_3 configuration, further consideration of this technique for output coupling was abandoned.

The Towles Coupler. Rooftop reflector "A" was fabricated as an output coupler by cementing a salvaged right-angle prism onto a germanium flat; a paper shim maintained the roof angle at 90° as the cement set. The prism surface had been overcoated with a thin layer of gold before cementing.

The Towles couplers always produced two output beams; an "axial" output along the axis of the gain medium and an "orthogonal" output perpendicular to that axis. These outputs were not due to two reflections of the same travelling wave (as occurred with the salt flat inserted into the cavity), but were separate samples of the two oppositely-directed travelling waves characteristic of ring resonators. The two outputs therefore had, in general, independent phase and intensity distributions. Reflector "A" was oriented with

the cavity radiation polarized perpendicular to the plane of incidence of the germanium.

The Towles coupler was therefore selected as the standard output configuration for the investigation of roof-resonator modes. From the data presented in Table II, neither orientation of the cavity polarization provided the correct output coupler reflectivity; it was, however, the best available choice.

IV. Experimental Procedures and Measurement Techniques

Intensity Distribution

During the investigation of the modes of the various roof-resonator configurations studied, a great deal of qualitative information about the near-field and far-field distributions of radiation intensity was obtained by observing the heating effect of the 10.6 μ radiation on fluorescent screens. These screens were activated by a small ultraviolet lamp held between 10 cm to 100 cm away and produced a greenish-yellow fluorescence which was clearly visible under subdued room illumination. Allowing the laser output to fall on the screen increased the local surface temperature at the point of incidence and therby quenched the fluorescence. The resulting dark spot revealed the presence of infrared radiation. Since the surface temperature was proportional to the laser beam intensity, the degree of darkening was also proportional to intensity and the variation of fluorescent intensity across the spot provided a qualitative measure of the intensity distribution of the beam.

The 8 screens used were each 7.5 cm square and provided a range of sensitivities from 0.1 watt/cm^2 to 100 watt/cm^2. The intensity range of each screen was such that a beam intensity which completely saturated (blackened) one screen caused a barely discernable darkening of the next less

sensitive screen. This feature often complicated the analysis of highly-structured beams (as were typical of the near-field outputs) and made necessary the use of two or more screens to adequately resolve the intensity variation.

The two most sensitive screens were constructed on substrates of very low thermal conductivity (in order to enhance the sensitivity). Consequently, the response time of these two screens to variations of intensity was limited to several seconds. This was not a problem when documenting mode structure, as the modes were fairly stable when the window heaters were turned off. It was a problem when the screens were being used to tune the alignment of the various cavities. The spatial resolution of the screens was very good, with some submillimeter details preserved. Fig 19 is an example of the photographs made of near-field and far-field spots:

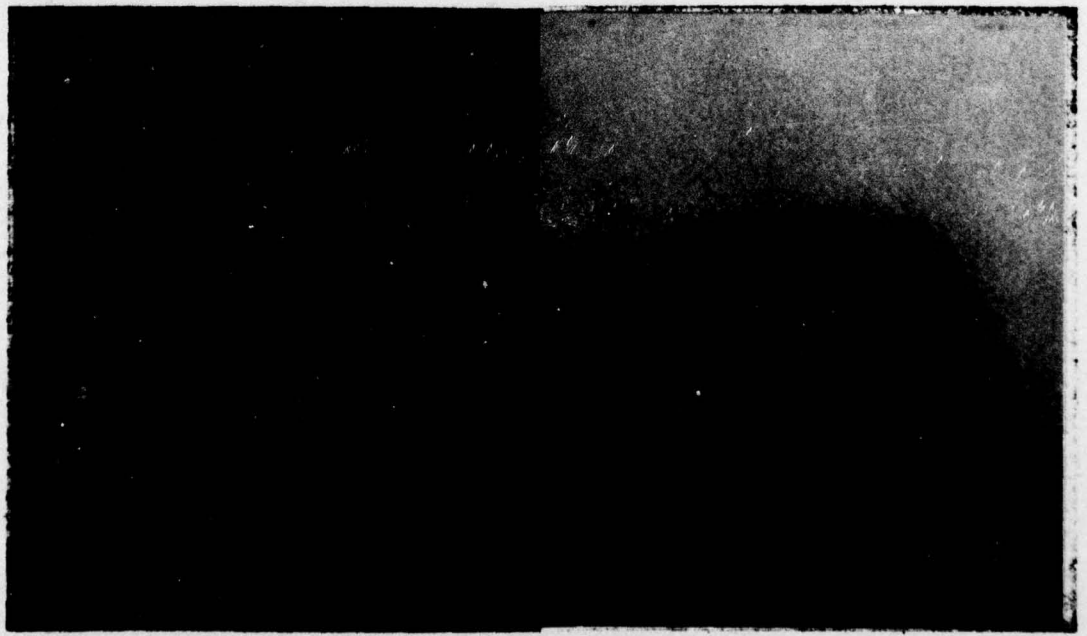

Fig. 19. Examples of near-field and far-field intensity distribution on thermal screens

Far-Field Intensity Profile

Quantitative determinations of the intensity distribution in the far-field of the roof-resonator output beams were made by scanning along their horizontal diameters with a sensitive Mercury-Cadmium-Telluride detector and recording the output. The detector and scanning system, described in Appendix D, provided two dimensional plots of intensity versus radial position. Peak intensity, spot size, and distortions of the shape of the distribution by overlapping modes were then determined from these plots. The sensitive area of the detector was only 0.25 mm square, so good spatial resolution was obtained. The detector was moved along its horizontal scan dimension by a travelling micrometer stage, which provided a precision for position determination of the order of 0.01 mm. The readout system degraded this precision by about a factor 3.

The detector had an intrinsically high bandwidth, but the recording system used was deliberately reduced in bandwidth to suppress noise fluctuations; the resulting bandwidth of the intensity scanning system was approximately 0.1 Hz. (ie, DC to 0.1 Hz). The micrometer stage was manually driven across its 24 mm range at a fairly constant rate of 0.3 mm/sec, taking 80 to 90 seconds for a single far-field scan.

The specific detectivity of the detector element (at 10.6 μ wavelength) was: $D^* = 3.7 \times 10^9$ cm $Hz^{\frac{1}{2}}$ W^{-2},

and its sensitive area $A_d = 6 \times 10^{-4}$ cm^2. The responsivity of the detector was experimately determined for the C.W. output of the roof-resonator by D.C. coupling the detector to a high-impedance electrometer and observing its reponse to a known flux. A value of R = 43 volts/watt was obtained by this technique, but a more meaningful calibration for interpreting the scan results is $\frac{1}{RA_d} = .037 \frac{\text{watts cm}^{-2}}{\text{millivolt}}$, since all the intensity scan data was recorded in units of millivolts. An example of the recorded far-field intensity scan is shown in Fig 20:

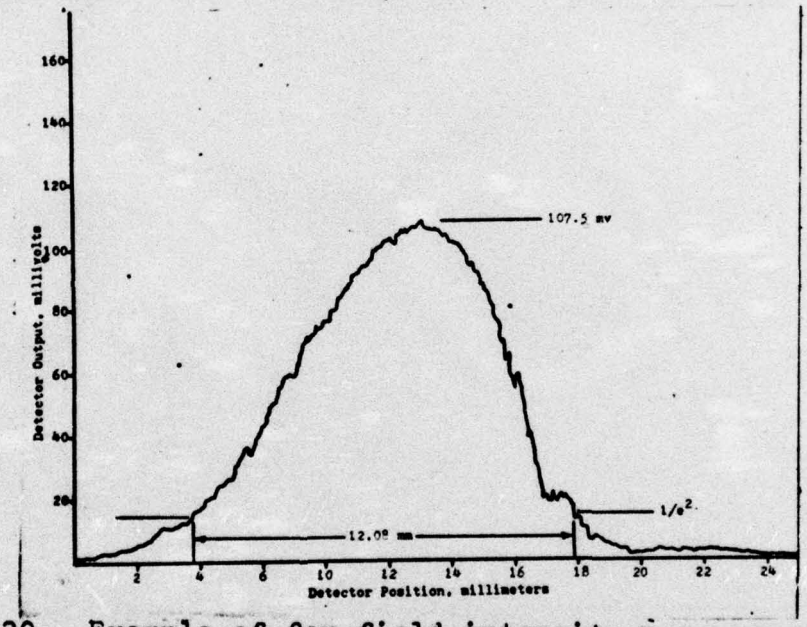

Fig. 20. Example of far-field intensity scan record

The "$\frac{1}{e^2}$" notation on the figure marks the point at which the intensity is e^{-2} times the peak value. The Half-width of the distribution at that level is then a measure of the divergence of the output beam according to Siegman's relation (Ref 25:314):

$$\theta = \frac{W_z}{Z} \qquad (16)$$

where W_z is the radius of the far-field spot to the $\frac{1}{e^2}$ intensity point and Z is the distance to the far-field point (taken as the focal distance of the far-field transform mirror).

In addition to beam divergence, the peak intensity and the symmetry of its distribution were considered in evaluating the several roof-resonator configurations investigated.

Mode Beating

The Mercury-Cadmium-Telluride detector used to scan the far-field intensity distribution also became the primary sensor for observing beating between the oscillation frequencies of the several modes of the roof-resonators. The observations were made by displaying the output of the detector on an RF frequency analyzer manufactured by the Singer Corporation. The analyzer, a model SPA-3000, provided an oscilloscope display of the frequency components of the detector output. Fig 21 is an example of the display, showing sharp vertical pips along the baseline at horizontal positions corresponding to the beat frequencies present in the detector output. The large pip on the left is the zero-frequency marker, aligned for convenience on the first graticle division of the oscilloscope display. The frequency dispersion of the SPA-3000 analyzer was variable, but was calibrated against the 5 MHz, 10 MHz, and 50 MHz

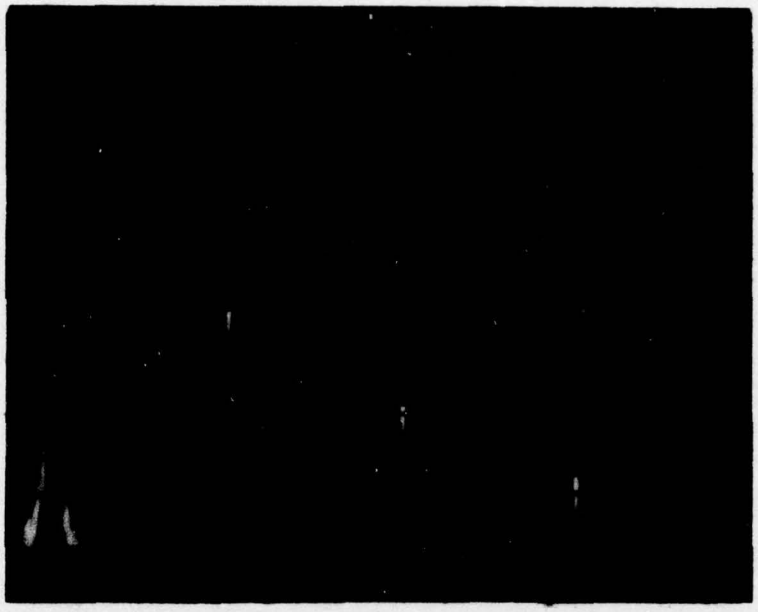

Fig. 21. Example of analyzer display showing multiple beat frequencies

outputs of a Fairchild model 718A Time Mark Generator. (The time mark generator used a thermally stabilized crystal as its interval frequency reference and was found to agree with the independently-calibrated reference of a digital frequency counter to 5 significant figures). A correction factor of 1.11 was thus determined for the 1 MHz/div, 3 MHz/div, and 10 MHz/div frequency dispersion settings, suggesting that the entire time base of the analyzer might be uncalibrated by that amount. All frequencies reported herein have been corrected to the higher value. For the 10 MHz/div dispersion of Fig 21, the observed frequencies are 17.22 MHz, 34.56 MHz, and 51.67 MHz. The differences between the oscillation frequencies of all the roof-resonator spatial modes were determined in this straightforward manner.

By activation of a phase-lock feature of the SPA-3000 frequency analyzer, dispersion was increased sufficiently to observe details of each beat frequency. Fig 22 is a multiple exposure of the display at 100 KHz/div dispersion:

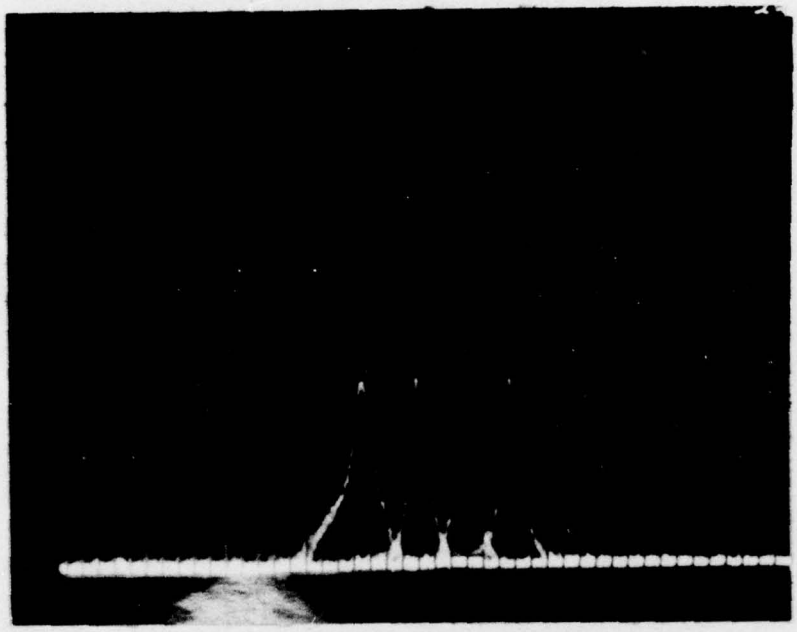

Fig. 22. Example of analyzer display showing beat frequency jitter

What appears as several separate pips in this figure was actually a "single" beat frequency as it randomly "jittered" about its mean value. This jitter was approximately ±0.2 MHz for all the roof-resonator configurations studied. By increasing the dispersion still further, the linewidth (and lineshape) of the individual beats was determined. Because the oscilloscope swept horizontally from left to right at a rate comparable to the jitter rate, the lineshape was somewhat distorted at these high dispersions. Specifically, the linewidth appeared shortened when a sweep occurred as the beat frequency was decreasing, (moving opposite the sweep) and was apparently lengthened during

periods of increasing frequency (moving with the sweep). Fig 23 is a multiple exposure at a dispersion of 30 KHz/div. The line appears Lorentzian, with a linewidth between these apparent values of 13 KHz and 39 KHz.

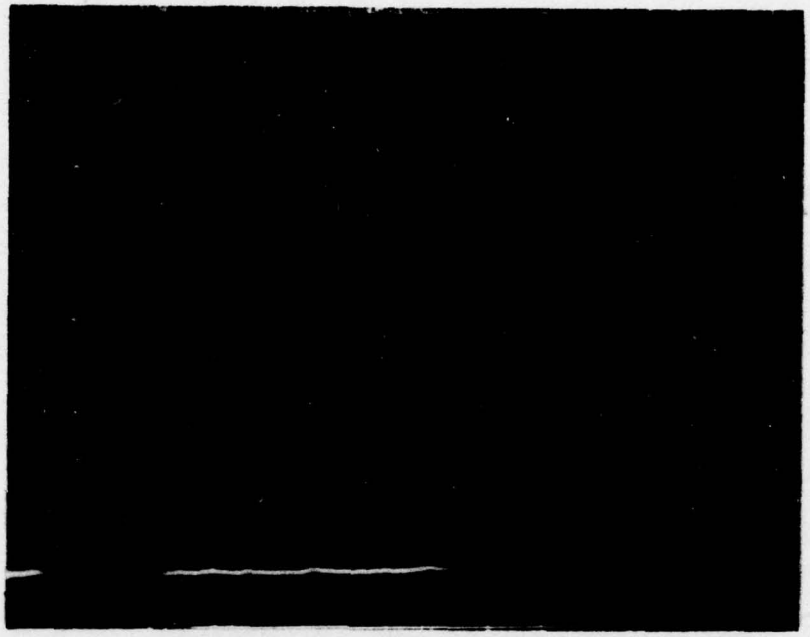

Fig. 23. Example of beat frequency lineshape

Misalignment Sensitivity

In order to provide still another quantity by which to judge the effectiveness of the various roof-resonator configurations, the Hg-Cd-Te detector was used to document variations in the peak intensity of the various far-field outputs as one of the roof-reflectors of each set was misaligned by known amounts. In all cases, the output reflector was kept fixed and the opposite reflector was misaligned about an axis perpendicular to its roof edges (since rotating about the roof edge had no effect on the propagation direction of the radiation in the cavity, as Chapter II showed). For each misalignment introduced, the

beam was re-positioned on the detector so that the new (misaligned) intensity distribution was maximized on its sensitive area. In this way, the peak intensity for each alignment was measured; detector output values were observed on Kiethley model 600A electrometer and manually recorded. Fig 24 is an example of the plot of a typical set of this data:

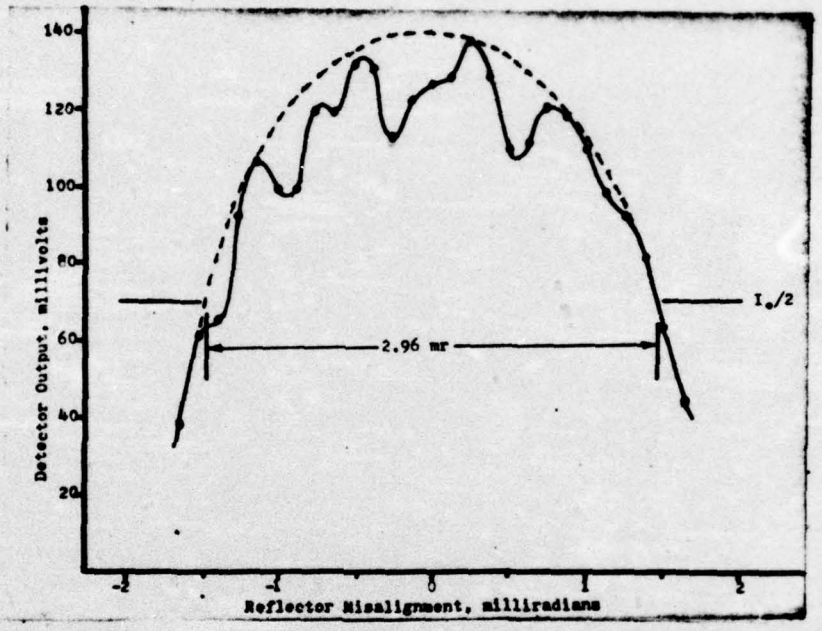

Fig. 24. Typical far-field intensity variation with roof-reflector misalignment

The data revealed a significant irregularity in intensity (this is the worst case) as the misalignment angle was changed. This may have been real or it may have been due to the difficulty of re-positioning the spot to its exact peak on the detector after each misalignment.

The dotted curve in Fig 24 represents an upper bound of the peak far-field intensities. The half-width of this "envelope" at its half-intensity points is taken as measurement of alignment sensitivity of intensity for the

several roof-resonators investigated. It represents the angle, $\delta\Phi$, through which the roof may be misaligned without changing the far-field intensity more than a factor 2.

The amount of re-positioning required to return the far-field intensity peak to the detector center provided a useful measure of the change in output angle of the beam for specific misalignments of the roof. (This measurement was not performed for all the roof-resonator configurations). A flat auxiliary mirror was used to direct the beam from the focusing mirror to the detector in the far-field plane; adjustments of this flat re-positioned the intensity peak on the detector after each misalignment. By recording the alignment of the flat at the end points of each data set (the outermost points plotted in Fig 24 for example) the total angle through which the output beam was deflected by the misalignment was measured. Analytically, the far-field beam deflection caused by an output angle change, $\delta\theta$, is

$$X = R \tan \delta\theta \qquad (17)$$

where R is the focal distance of the mirror; that same deflection is caused by adjusting the folding flat through a compensating angle, $\delta\gamma$,

$$X = S \tan 2(\delta\gamma) \qquad (18)$$

where S is the distance from the flat to the far-field plane. Therefore the equality follows

$$R \tan \delta\theta = S \tan 2(\delta\gamma) \qquad (19)$$

from which the change in output angle, $\delta\theta$, was determined.

This angle was then divided by the total angle through which the roof-reflector was misaligned between the same endpoints to obtain $\frac{\delta\Theta}{\delta\varphi}$, the misalignment sensitivity of output angle for the several roof-resonator configurations studied.

V. Flat-90° Roof-Resonator Investigations

Experimental Conditions

The flowing gas discharge tube described in Appendix A was operated under the "standard operating configuration" established in chapter III. A flat, gold-coated pyrex mirror and the 90° Towles coupler (Reflector "D" described in Appendix C) were placed at opposite ends of the discharge tube, each 100 cm from the midpoint of the discharge electrodes. (This arrangement was called the F-D resonator.)

The germanium surface of Reflector "D" was 45° to the tube axis ± 1.5 milliradians, and its roof edge was vertical. This arrangement produced two output beams from the resonator: the beam parallel to the resonator axis was called the "axial" output and represented the travelling wave propagating in a clockwise direction around the resonator (when viewed from above); the travelling wave propagating in a counterclockwise direction was reflected from the gold surface of Reflector "D" before being transmitted through the germanium at a right angle to the axis, and was therefore called the "orthogonal" output.

The orthogonal output was focused by a concave mirror of 453 cm focal length and directed into the far-field plane by an auxiliary "folding flat". The Hg Cd Te scanning detector (described in Appendix D) was positioned in the far-field plane to measure the intensity of the

orthogonal output. The arrangement of optical components is diagrammed in Fig 25:

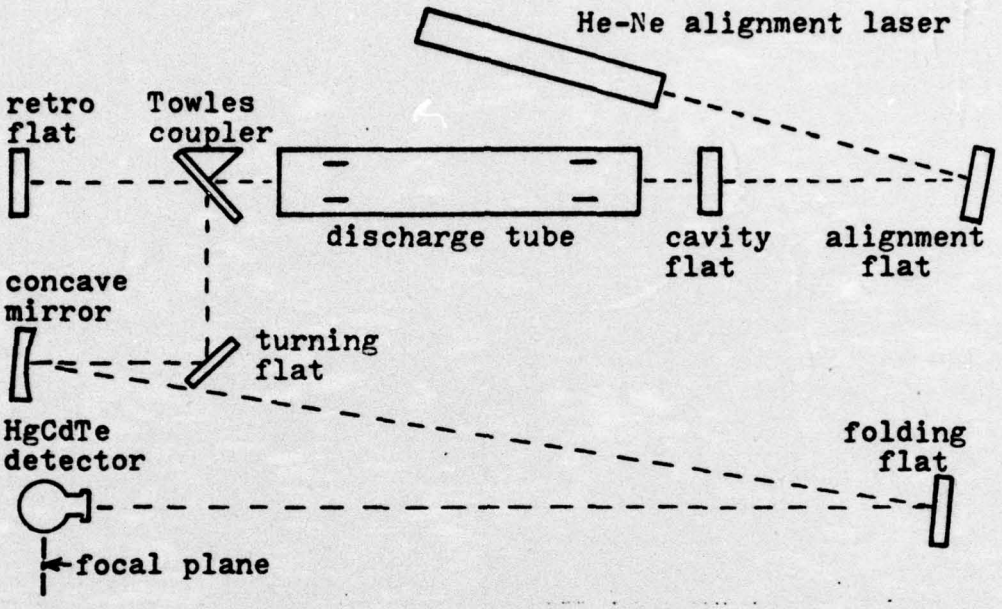

Fig. 25. Optical layout for F-D resonator investigation

Variables

During this investigation of the F-D resonator, output parameters were measured for two directions of polarization in the cavity; parallel to the roof-edge of the Towles coupler (and hence perpendicular to the plane of incidence of the germanium), and perpendicular to that roof edge. (Cavity polarization was changed by rotating the Brewster windows about the tube axis.) The parallel case was designated F-D$_{//}$, and, by calculation, provided 51.7% transmissivity (recall T(opt)=57%). The perpendicular case was called F-D$_{\perp}$ and transmitted 76.6% of the cavity radiation. Clearly the F-D$_{//}$ configuration should produce a greater output power. The horizontal position of the roof edge of Reflector "D" with respect to the axis of the

discharge tube was also changed during this part of the study. By moving the reflector slowly across the tube axis, three positions were found which could be distinguished by unique shapes (on the thermal screens) of the far-field spots of the axial and orthogonal outputs. With the roof edge of reflector "D" in the first position (called the "Ge" position because the discharge tube axis intersected the Towles coupler at its germanium surface), the far-field spot of the axial output collapsed to a circle and its peak intensity was maximized (while the far-field spot of the orthogonal output elongated in the horizontal direction). With the roof-edge of "D" in the "Au" position (so called because the axis of the gain medium intersected the gold surface of the Towles coupler), it was the orthogonal output whose far-field spot became symmetric and intense while that of the axial output smeared out and became less intense. The third position, call the "M" position, was exactly midway between the Au and Ge positions. It produced far-field spots of the two output beams which were the same size and shape - slightly elongated in the horizontal dimension. The Au and Ge positions of the roof-edge were exactly 3 mm apart, and the M position placed the roof edge exactly on the axis of the gain medium (allowing for refractive displacement at the Brewster windows of the discharge tube).

The cavity flat, reflector "F", was adjusted to various alignments during the investigation of the F-D$_{//}$ and F-D $\perp$

resonator configurations. This alignment has several effects, and two are reported in the results for this resonator. The first effect of misaligning reflector"F" was to change the mode structure of the cavity, an effect for which only qualitative results were determined. The second effect of misaligning the cavity flat was to decrease the intensity of the far-field spot (a quantified effect). Both vertical and horizontal misalignment sensitivities were measured: the results for vertical misalignment refer to a rotation of reflector "F" about a horizontal axis, so that its normal continued to intersect the roof edge of reflector "D"; the results for horizontal misalignment refer to rotations about the vertical axis of reflector "F", so its plane of incidence is always orthogonal to the roof edge of reflector "D".

Results

Operation at Maximum Power. Initial operation of the F-D$_{//}$ resonator revealed that the power output of the laser was a sensitive function of the alignment of reflector "F". With the roof of reflector "D" vertical and centered on the axis of the gain medium, reflector "F" was tuned for maximum power in the far-field of the orthogonal output. At this setting of the cavity-flat alignment, the power of both axial and orthogonal output beams was equal and maximized. (This observation was verified for the D$_{\perp}$ polarization configuration also). With this alignment, the near field output appeared as shown in Fig 26:

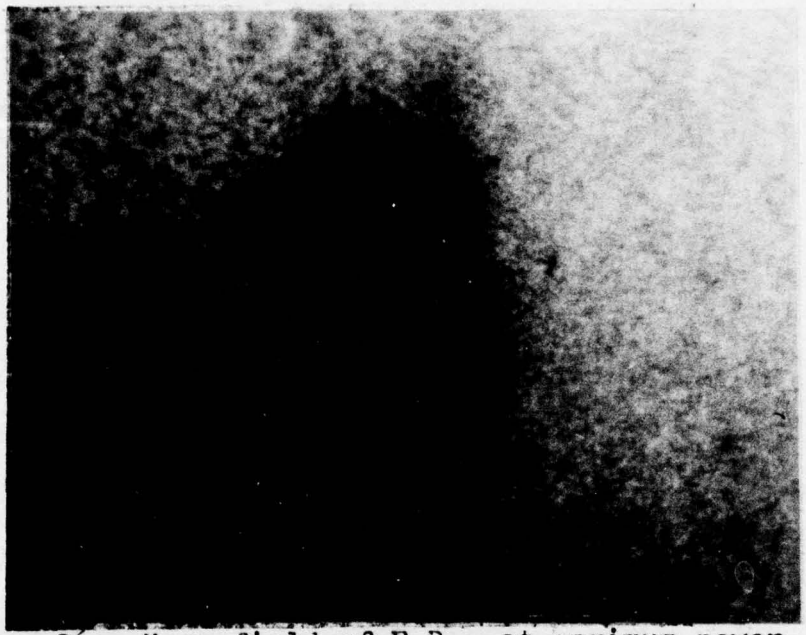

Fig. 26. Near field of F-D$_{//}$ at maximum power

In the far-field, this max-power alignment produced peak intensities for the F-D$_{//}$ and F-D$_{\perp}$ orthogonal outputs of 3.33 w/cm^2 and 5.59 w/cm^2 respectively. The corresponding beam divergences were 1.33 mr and 1.40 mr. The actual distributions were similar for polarization parallel and perpendicular to the roof edge; the F-D$_{\perp}$ orthogonal far-field is shown in Fig 27. A gaussian distribution with the same peak and e^{-2} width is shown by the dashed curve for comparison. When the Hg Cd Te detector was positioned at the center of this distribution, an intermittant beat frequency of 10.5 MHz was observed. Fig 28 shows the sinusoidal structure of this beat as displayed on an ordinary (time domain) oscilloscope. Occasionally a beat was observed with frequency 17.5 MHz.

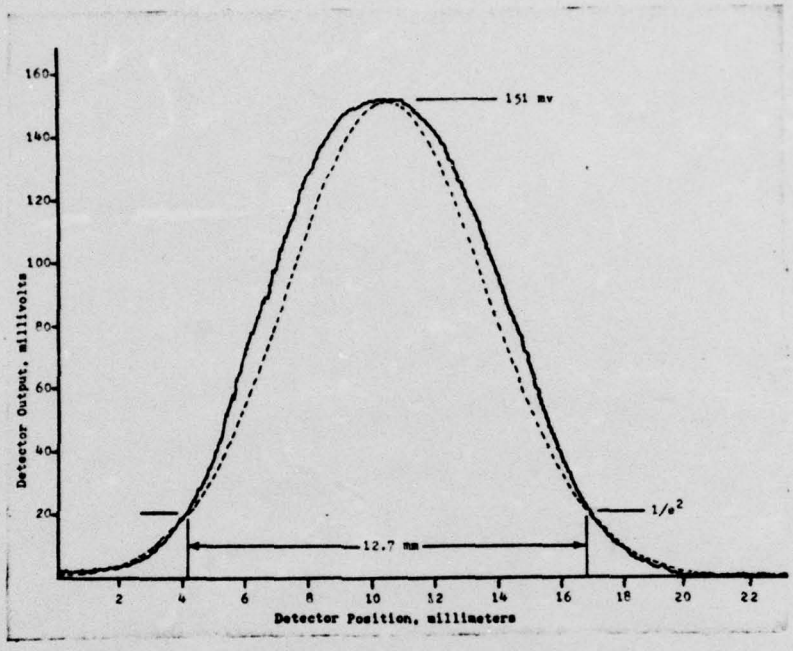

Fig. 27. Intensity distribution for F-D$_{\perp}$ at maximum power

Fig. 28. Beat frequency of F-D$_{//}$ at maximum power

Multimode Operation. With the beats between the modes of the F-D$_{//}$ resonator displayed on the frequency-domain oscilloscope of the SPA-3000 analyzer (see Chapter IV), the cavity flat was rotated from its maximum-power alignment. (All the observations of mode beating described here for the F-D$_{//}$ configuration were later verified for the horizontal polarization of the F-D $\perp$ case). It was observed that the frequencies of the beats were continuously tunable between 11 MHz and 15.5 MHz, and between 22 MHz and 31 MHz. The higher-frequency beat was always twice that of the fundamental, and both were most stable and had the highest amplitude near the center of their range. Fig 29 is a multiple exposure of the tuning variation of the lower-frequency beat:

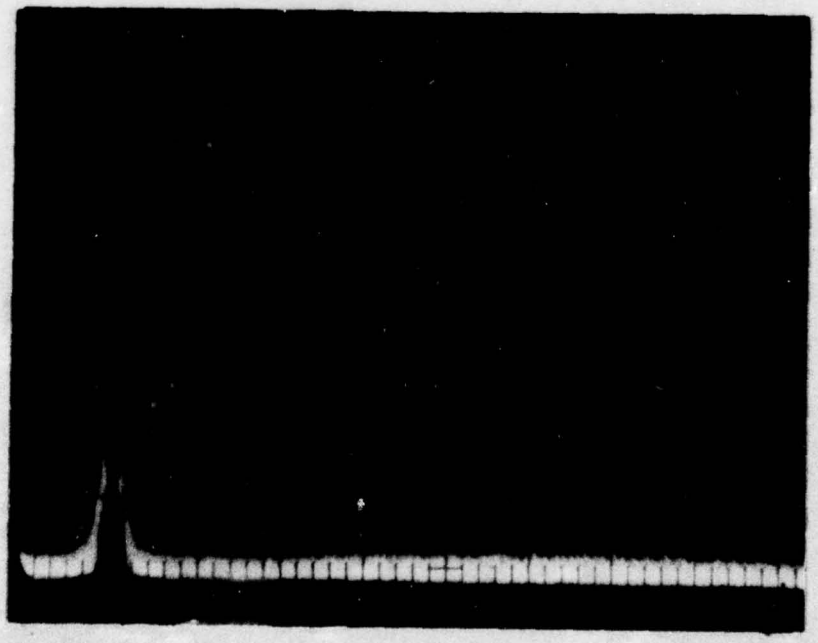

Fig. 29. Limits of beat frequency variation by cavity alignment

Very rarely a beat would appear at 8.33 MHz as reflector "F" was tuned over this range, but no beats were ever observed between 8.33 MHz and 11 MHz. The appearance of the 8.33 MHz beat was too fleeting to determine whether its frequency could be changed by tuning the flat.

The cavity flat was tuned to the alignment which produced the most stable, highest amplitude beats (12.5 MHz and 25 MHz); jitter and beat frequency bandwidth were verified (as described in chapter IV) to be ± 0.2 MHz, and 21.5 KHz respectively. At this alignment of reflector "F" (called the multimode alignment), the near-field of the orthogonal output appeared as shown in Fig 30:

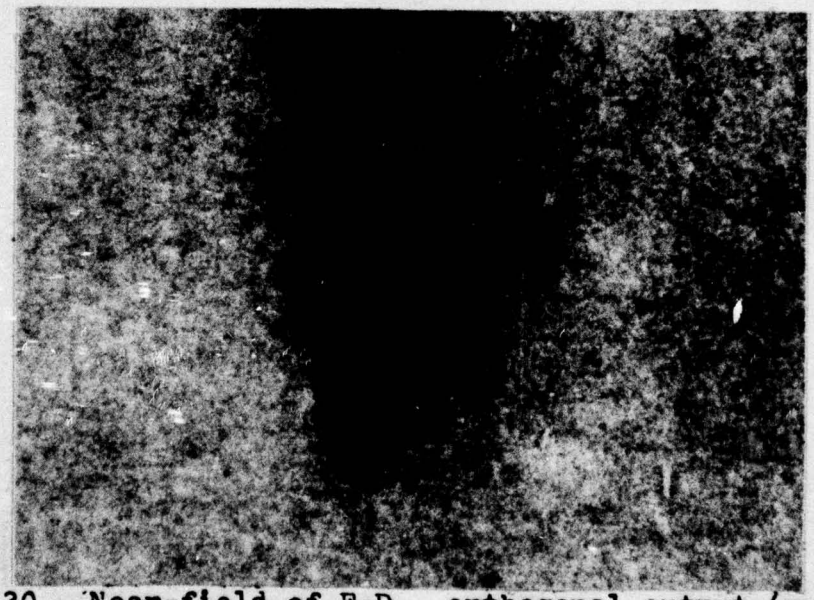

Fig. 30. Near-field of F-D$_{//}$ orthogonal output (multimode)

The far-field intensity distribution at this alignment was significantly spread and reduced in intensity, as the example of Fig 31 shows:

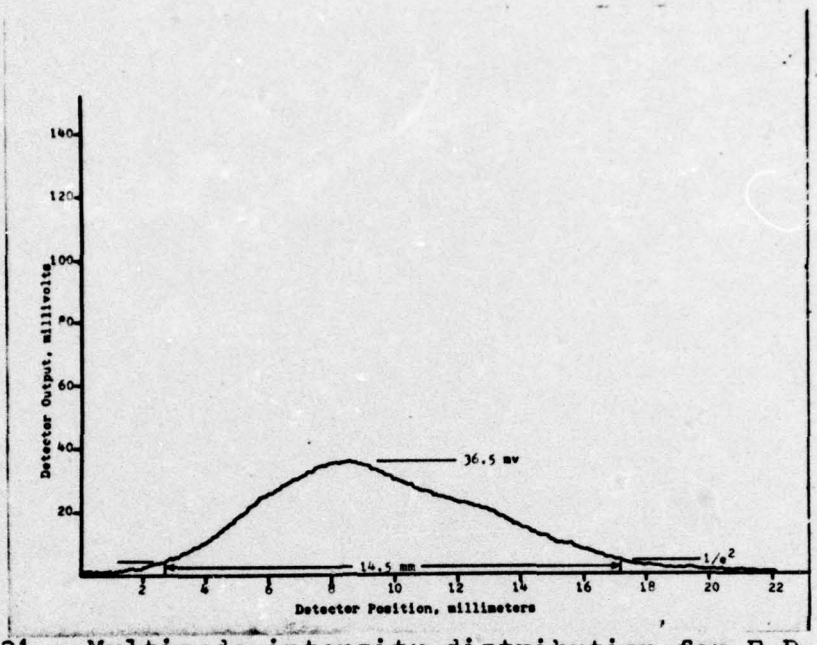

Fig. 31. Multimode intensity distribution for F-D

The peak intensity and beam divergence for the F-D$_{//}$ (vertical polarization) configuration were $I_o = 1.33$ w-cm^{-2} and $\theta = 1.60$ mr respectively. The same parameters for the F-D$_{\perp}$ resonator were $I_o = 0.84$ w-cm^{-2} and $\theta = 1.66$ mr.

Misalignment Effects. By rotating reflector "F" clockwise about a vertical axis an amount 1.4 mr, the orthogonal output was reduced in intensity while that of the axial output was practically unchanged (further rotation in this direction reduced the intensity of the axial output also). At this rotation limit, the orthogonal output was completely suppressed by introduction of a 9.0 mm diameter aperture placed 4.3 cm from reflector "F" and concentric with the discharge tube axis to ±0.5 mm. The aperture caused a small but noticeable reduction in the

intensity of the axial output at this alignment.

Misalignment of the cavity flat by an amount 1.27 mr on either side of the position which maximized the intensity of the orthogonal output reduced that intensity by a factor 2; the horizontal misalignment sensitivity for the F-D$_{//}$ resonator was thus taken to be $\delta\Phi = \pm 1.27$ mr. This same sensitivity to vertical misalignment of Reflector "F" was $\delta\Phi = \pm 0.19$ mr.

Output Coupler Position. The roof edge of the Towles coupler was horizontally translated across the discharge tube axis as described in the second section of this chapter. Only the effect on the far-field intensity distribution of the orthogonal output was measured for this variable. All the distributions were symmetric about I_o, and the resulting peak and divergence are summarized in table III:

Table III
Peak Intensity and Divergence for
Several F-D Resonator Configurations

Configuration	Roof Position	I_o	θ
		w-cm^{-2}	mr
F-D$_{//}$	Ge	2.15	1.78
F-D$_{//}$	M	3.98	1.33
F-D$_{//}$	Au	5.00	1.25
F-D$_{\perp}$	Ge	2.46	1.56
F-D$_{\perp}$	M	3.13	1.34
F-D$_{\perp}$	Au	4.74	0.856

Superposition of Outputs. Following a technique common in ring-resonator technology, an attempt was made to return the axial output to the resonator and therby enhance the orthogonal output. This was accomplished by aligning the retro-mirror (see Fig 25) until the far-field spot of the beam reflected from the rear germanium surface of reflector "D" was superimposed on the far-field spot of the orthogonal output. This caused the axial output to be reflected back into the cavity (through the germanium) along the direction of the travelling wave which produced the orthogonal output.

When the far-field spots were close together, their combined power was approximately twice that of either single output. As the spots were moved closer to coincidence, interference effects became dominant; at the alignment which would have superimposed the spots, both beams disappeared and no power could be measured in the far-field.

Analysis

Modes. The results of the intensity scan at the max-power alignment indicate that the F-D resonator behaves much like a flat Fabry-Perot cavity which has been folded by the roof reflector. The near-field photo indicates that the path of the beams in the cavity is very close to the axis, so that the rays are confined to the semicircular aperture formed by the roof edge and the inner edge of the electrode. Since the vertical and horizontal dimensions of this aperture are respectively the diameter and radius of the electrodes, a greater difference is expected in the horizontal direction,

as observed.

Fig 28 indicates that, even when perfectly aligned, the F-D resonator supports some spatial modes other than the so-called "axial" mode which propagates in the direction of the resonator axis; these weak modes have propagation directions slightly off axis. Because the diffraction effects of the cavity aperture are large in this case (of the order of 1mr), the separate mode directions are not resolved in the far-field; higher order spatial modes only smear out the intensity distribution.

When the cavity is misaligned more higher-order modes begin to oscillate and with greater intensity. Fig 31 shows how the presence of these modes at large propagation angles spreads out the far-field intensity distribution.

The first non-axial mode supported by this resonator is the "fundamental ring" mode depicted in Fig 5 (which is characterized by a mode number of 1 and designated the first odd mode). As was pointed out in section II, the phase-repetitive path length for this mode is the distance of one round trip around the cavity. This distance is found by inspection of Fig. 5 to be (approximating cos α by the first two terms of the expansion):

$$D_1 = \frac{2L}{\cos \alpha} = 2L \left(1 + \frac{\alpha^2}{2}\right) \qquad (20)$$

where the subscript refers to mode #1.

The path lengths for the first few higher modes are

found by similar trigonometric consideration:

$$D_2 = 2L + \frac{2L}{\cos 2\alpha} = 2L\left(1+1+\frac{4\alpha^2}{2}\right) = 4L\left(1+\alpha^2\right) \qquad (21)$$

$$D_3 = \frac{2L}{\cos\alpha} + \frac{2L}{\cos 3\alpha} + \frac{2L}{\cos\alpha} = 2L\left(1+\frac{\alpha^2}{2}+1+\frac{9\alpha^2}{2}+1+\frac{\alpha^2}{2}\right)$$

$$= 6L\left(1+\frac{11}{6}\alpha^2\right) \qquad (22)$$

$$D_4 = 2L + \frac{2L}{\cos 2\alpha} + \frac{2L}{\cos 4\alpha} + \frac{2L}{\cos 2\alpha} = 8L\left(1+3\alpha^2\right) \qquad (23)$$

It is this difference in path length which produces the slightly different frequencies of each mode.

Since the roof angle of reflector "D" is 90° (within a fraction of 1 milliradion), and since the finite size of the roof edge discontinuity (about 0.38 mm) does not allow an infinitesimally narrow mode volume, a strictly geometric explanation cannot account for the existence of any of the higher order modes (higher, that is, than the "axial" mode of the mode number zero and path length $D_o = 2L$. The zeroth mode reflects at normal incidence from the flat, makes one reflection at each surface of the roof reflector, and returns normal to the flat without intersecting itself). The mechanism postulated for the propagation of modes of order 1 or higher is diffraction: as the cavity radiation passes the electrode surface or the roof edge some of its energy is diffracted into angles of the order of milliradians. This energy strikes the flat and returns to the roof with enough gain to overcome the output losses and provide, by diffraction alone, sufficient energy to maintain a stable mode in the cavity.

The oscillation frequency of the $m^{\underline{th}}$ mode (of the $q^{\underline{th}}$ axial mode) is:

$$f_{qm} = \frac{q\ c}{n_o\ D_m} \tag{24}$$

where $\frac{c}{n_o}$ is the velocity of propagation in the cavity medium, and D_m is the round-trip path length of the $m^{\underline{th}}$ mode.

If another mode, qp, is oscillating in the cavity with the same axial mode number, q, then its frequency is:

$$f_{qp} = \frac{q\ c}{n_o\ D_p} \tag{25}$$

and the difference (beat frequency) is:

$$\Delta f_{mp} = \frac{qc}{n_o}\left(\frac{1}{D_m} - \frac{1}{D_p}\right) = \frac{qc}{n_o}\left(\frac{D_p - D_m}{D_p D_m}\right) \tag{26}$$

In order for the higher order modes to continue oscillating in the cavity, the radiation diffracted during each pass must be in phase with the radiation propagating along the geometric path. This requires that the paths of the higher order modes be phase-repetitive, not just upon their own closed path, but at the end of every round trip of the cavity. The so-called "interferometric path-length", the length which determines the resonant frequency of each mode, is therefore $\frac{1}{m}^{\underline{th}}$ the distance computed in equations (20) through (23). If the resulting "interferometric path-length" is applied to equation (26), the beat frequencies are:

$$\Delta f_{02} = \frac{qc}{n_o} \frac{2L\alpha^2}{4L^2+4L^2\alpha^2} \approx f_o\alpha^2 \qquad (27)$$

$$\Delta f_{04} = \frac{qc}{n_o} \frac{6L\alpha^2}{4L^2+12L^2\alpha^2} \approx 3f_o\alpha^2 \qquad (28)$$

$$\Delta f_{24} = \frac{qc}{n_o} \frac{4L\alpha^2}{4L^2+\frac{22}{3}L^2\alpha^2+22L^2\alpha^2} \approx 2f_o\alpha^2 \qquad (29)$$

where $f_o = \frac{qc}{2n_oL} = 2.82 \times 10^{13}$ Hz

If, on the assumption that the above frequency differences, (Δf_{02}, Δf_{04}, Δf_{24}) correspond to the most stable measured beat frequencies of the F-D resonator of 8.33 MHz, 25 MHz, and 12.5 MHz respectively, an effective roof angle is computed by the relation

$$\alpha^2 = \frac{\Delta f_{mp}}{k_{mp}} \left(\frac{qc}{2n_oL}\right)^{-1} = \frac{\Delta f_{mp}}{k_{mp}f_o} \qquad (30)$$

where k_{mp} are the factors 1, 3, 2 computed above.

For $q = 3.77 \times 10^5$,

$$\alpha_{02} = .544 \text{ mr}$$
$$\alpha_{04} = .543 \text{ mr} \qquad (31)$$
$$\alpha_{24} = .471 \text{ mr}$$

This is a very reasonable diffraction angle for a 10.6μ wave through the M aperture; the diffracted intensity at this angle is 0.67 times the intensity of the geometrical (axial) ray. The close agreement of values for α tends to confirm the assumption that the beating observed is the result of interference between the m = 0, m = 2, and m = 4 modes of the resonator. The even modes are probably favored since they each have two reflections per pass at

normal incidence to the cavity flat. The resulting mode paths of the F-D rooftop resonator are as depicted by Fig 32:

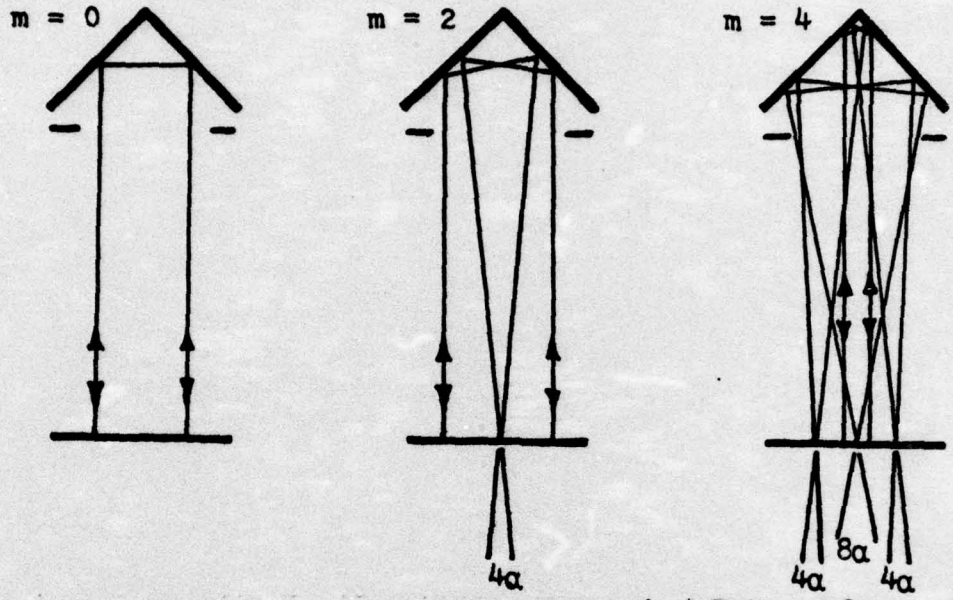

Fig. 32. Probable modes of the operating F-D roof resonator

The observed frequency shift which occurred when reflector "F" was misaligned is simply the effect of changing the angle which the diffracted radiation takes as it leaves reflector "F" (ie, it changes the effective roof angle, α, of the reflector and by equation (30), varies Δf).

The beam divergence of the m = 4 mode is $\theta = 4\alpha \approx 3$ mr. If only the m = 4 mode had been oscillating during the multimode operation, the observed divergence would have been greater than the 1.66 mr measured (Fig 31) In fact, the m = 0 and m = 2 probably contained the majority of the energy, and thereby maintained the far-

field intensity in a narrower distribution.

Polarization. The effect on intensity and divergence caused by changing the direction of polarization of the cavity radiation is summarized in table IV (polarization direction indicated with respect to the roof edge):

Table IV

Summary of Intensity and Divergence for F-D Roof Resonator Operation.

Flat Alignment	Roof Position	Polarization	I_o, w-cm^{-2}	θ, mr	$\frac{I_{o//}}{I_{o\perp}}$	$\frac{\theta_{//}}{\theta_{\perp}}$
Multimode	M	//	1.33	1.60	1.58	0.96
		$\perp$	0.84	1.66		
Max Power	M	//	3.33	1.33	0.60	0.95
		$\perp$	5.59	1.40		
Axial	Ge	//	2.15	1.78	0.87	1.14
		$\perp$	2.46	1.56		
Axial	M	//	3.98	1.33	1.27	0.99
		$\perp$	3.13	1.34		
Axial	Au	//	5.00	1.25	1.05	1.46
		$\perp$	4.74	0.86		

There is no clear indication that either polarization gives superior performance under all the operating conditions investigated (the average ratios of intensity and divergence are 1.07 and 1.10 respectively). In one case, however, the parallel polarization is clearly superior: in multimode operation, the intensity is significantly greater than that provided by horizontally polarized radiation. This is probably because, at the larger angles which the higher-

order modes make with the Brewster windows in the horizontal plane, the Fresnel reflection losses are greater with the window plane of incidence horizontal (ie, the windows are more angularly selective in their plane of polarization).

This effect also explains the improved beam divergence of the perpendicularly polarized output with the roof position optimized for the orthogonal output (ie, Au position). This improvement because of window selectivity probably occurs at all positions of the roof edge, but is dominated by diffraction effects at the other positions. The improvement in divergence is not without a penalty in intensity, however, since the mode volume is reduced with the greater angular selectivity.

Output Coupler Position. The effect of the output coupler position just mentioned is of great practical significance for rooftop resonators. There is clearly a favored mode path for the radiation in the gain medium; if the roof edge is translated by an amount which moves the mode path close to a diffraction edge, the output deteriorates significantly. Practical lasers must have large enough Fresnel numbers to allow the mode paths to oscillate without interference.

In the present case, the inside edge of the discharge electrode and the roof edge form apertures only 5.5 mm wide when the Towles coupler is in the M position. Translation of 1.5 mm to the Au position opens the aperture on one side of the orthogonal output to 7 mm, but contracts the other output to only a 4 mm aperture (thereby causing the observed

degradation in divergence and intensity). There is also significent diffraction of the portion of the favored (orthogonal) wave which is reflected back into the gain medium through the 4 mm aperture - so much in fact that the transverse intensity distribution of the mode is no longer gaussian. Apparently the interaction with the 4 mm aperture diffracts the beam to such an extent that when it has returned to the output coupler after passing through the 4 meter (round trip) gain path, its spot size is very much larger than the 7 mm output aperture. The resulting Fraunhoffer diffraction into the far-field is then characteristic of a rectangular aperture illuminated by a plane wave (Ref 20:393, 565 et. seq.).

The far-field intensity distribution of a plane wave through a rectangular aperture is best described by:

$$I = I_o\left(\frac{\sin kqa}{kqa}\right)^2 \qquad (32)$$

where k is the propagation constant, $\frac{2\pi}{\lambda}$, a is the half-width of the aperture, q is the direction cosine of the diffracted radiation, $\frac{\text{position}}{\text{distance}}$.

This function is plotted as a dashed curve in Fig 33, which also shows secondary intensity maxima at the 3.5 mm and 18.5 mm detector positions of the intensity distribution for the orthogonal output of F-$D_{\perp}$ in the Au position.

Since the electrode aperture and the roof edge are not at the same position along the resonator axis, their effective aperture is larger than 7 mm. The half-width of the aperture used for the plot in Fig 33 was actually

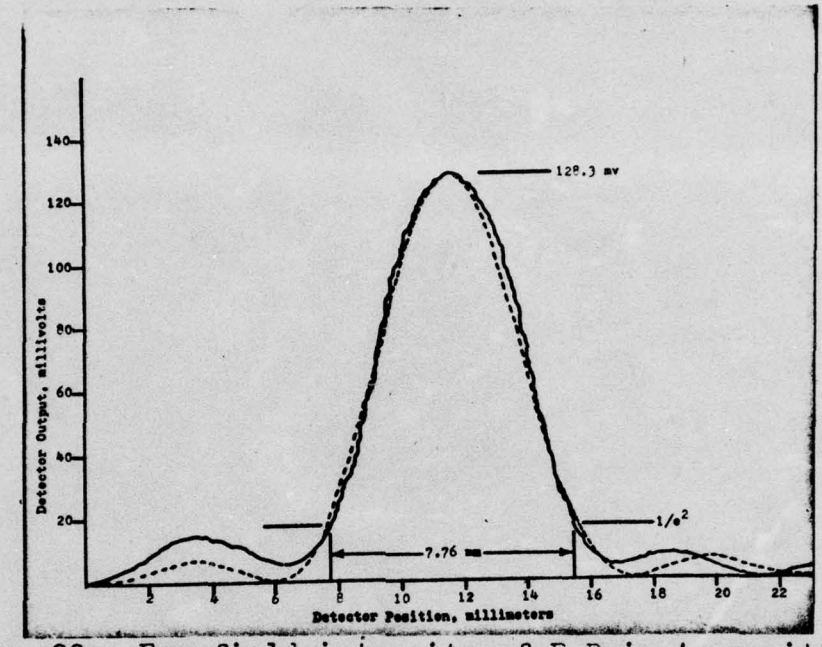

Fig. 33. Far-field intensity of F-D in Au position

a = 4.22 mm, which is the projection of the electrode radius onto the reflector surface. As can be seen from Fig. 33, the secondary maxima do not have exactly the same amplitudes and positions as the plot of equation (32), but the fit is close enough to support the above interpretation of output coupler position effects.

Unexplained Effects. No adequate explanation has been formulated for the suppression of the orthogonal output by the 9 mm aperture when the flat was misaligned by an angle of 1.4 mr, or the disappearance of the axial and orthogonal far-field spots when they were superimposed.

VI. Two 90° Roof Reflectors

Experimental Conditions

The conditions under which this phase of the roof-resonator investigation was conducted were those which prevailed during the Flat-90° Roof experiments (see chapter V). The only exception was that the cavity flat, reflector "F", was replaced with a totally-reflecting 90° rooftop, reflector"C". (The construction and specifications of all the rooftop reflectors used in this study are described in Appendix C.) Reflector "D", the partially-transmitting 90° rooftop was retained as the cavity output coupler, and was placed in the cavity exactly as it had been for the F-D configuration (ie, roof edge vertical and germanium surface 45° to the tube axis.) The "orthogonal" and "axial" outputs were the same for both phases of the study, and the orthogonal output was again chosen for far-field intensity distribution measurements. The arrangement of optical components remained as diagrammed in Fig 25 (chapter V) except that reflector "C" replaced the cavity flat. The polarization of the cavity radiation was maintained horizontal (ie, perpendicular to the roof edge of the output coupler) during this entire phase of the investigation.

Variables

During the investigation of the two 90° roof reflectors as resonator elements only three major parameters were varied: the orientation of the roof edges about the axis of the

discharge tube, the transverse positions of the roof edges relative to the tube axis, and the alignment angle between the roof edge of the total reflector and the tube axis. Throughout this chapter, the terms "orientation", "position", and "alignment" have these meanings.

Only two orientations of roof edges about the tube axis were thoroughly investigated: the cases where the roof edges were mutually perpendicular were identified symbolically as C⊥D, and the cases for which the roof edges were practically parallel were noted as C//D. Operation of the resonator at other than these (unique) roof orientations was briefly observed but no measurements were made. The setting of the orientation angle was relatively imprecise: a value of ± 20 mr is the smallest probable error which can be ascribed to the perpendicularity or parallelism of the roofs.

The transverse position of both roof edges relative to the tube axis was changed during this phase of the investigation. Reflector "D" was used in the same three positions as had been identified as unique during the F-D studies: the Au position minimized the horizontal spread of the far-field spot of the orthogonal output and maximized its intensity. the Ge position did the same for the axial output, and the M position was exactly in between. The roof edge of reflector "C", being mounted approximately 1 cm from the rotation axis of its support, was translated across the tube axis by micrometer adjustments of rotation. The

resulting rotations of reflector "C" about its roof axis had no effect on the directionality of the cavity radiation, as explained in chapter II. Five positions of the roof of reflector "C" were found to produce unique effects under certain circumstances. These positions were identified by their distance from the axis in millimeters (ie, 0, 0.3, 0.5, 0.6 and 1.0 are the identifying symbols for this variable). All the positions thus identified were above (vertically up from) the axis except the 1.0 position, which was horizontally translated (and the 0 position which was on the axis).

The alignment of the roof edge of reflector "C" was the third variable for this phase of the roof-resonator study. The roof of the total reflector was rotated about a horizontal axis (for C//D orientations) and about a vertical axis (for C⊥D cases) to study the effect of misalignment on far-field intensity and to change the beat frequency of the cavity modes.

Results

All the observations and measurements relating to a particular combination of roof edge orientation and output coupler position are reported together. The appearance of the near- and far-field spots, the far-field intensity distributions, and the beat frequencies between modes are the major observables common to each of the combinations. Where applicable, the misalignment sensitivity of peak intensity and beam output direction is also reported.

C⊥D Resonator, M Position, "C" Aligned. The vertical position of the roof of reflector "C" was adjusted about its aligned position until the power of the orthogonal output was maximized. Since the vertical adjustment required to maximize the power (.033 mm) was smaller than the alignment imprecision, the new position of the roof was assumed to be on the axis of the discharge tube. With this alignment of the reflectors, the near-field and far-field spots appeared as shown in Fig 34:

Fig. 34. Near-field and far-field spots for aligned C⊥D resonator (M output position)

At this alignment, Reflector "D" was rotated about its roof edge from approximately 40° angle of incidence onto the germanium surface to nearly 50°. No change in either intensity or shape of the far-field spot was observed.

Three separate scans were made of the intensity distribution in the far-field of the output of this

configuration. The scans were not made consecutively: other experiments (involving different alignments of the total reflector and different positions of the output coupler) were performed in the interim.

The three peak intensities measured were 3.33 w-cm^{-2}, 3.12 w-cm^{2}, and 3.66 w-cm^{-2}; the three associated beam divergence values were 1.33 mr, 1.37 mr, and 1.28 mr.

A successful attempt was made to combine the axial and orthogonal outputs by aligning the retro-flat (see Fig 25) to superimpose the two far-field spots. At the best alignment (maximum intensity), the intensity distribution of the combined spot was scanned. The peak intensity was measured as I_o = 5.33 w-cm^{-2} and overall divergence angle as θ = 1.41 mr.

C | D Resonator, M Position, "C" Misaligned. The roof edges of reflector "C" was translated vertically 0.6 mm above its aligned position. The resulting near-field and far-field outputs are shown in Fig 35. A horizontal intensity scan through the upper lobe of the far-field spot indicated a peak intensity of I_o = 3.18 w-cm^{-2} and a horizontal divergence of θ = 1.33 mr. The vertical separation of the lobes is slightly smaller than their horizontal dimension, so the angular separation of the lobes is taken to be about one milliradian. No beat frequencies were observed when this mode was oscillating.

When the roof edge of reflector "C" was positioned 0.3 mm above the axis, the far-field spot drifted from the

Fig. 35. Near-field and far-field spots for C⊥D Resonator misaligned by 0.6 mm (M output position)

pure-mode appearance of Fig 35 to the pure-mode appearance of Fig 34 and back with a transition period of several seconds. During the transition, the spot became a formless smudge and a beat frequency of 19.33 MHz was observed on the frequency analyzer. The transition between the single-lobe mode and the double-lobe mode was controlled by rotating reflector "D" about its (vertical) roof axis: at misalignment angles of $(2q + \frac{1}{2})$ 1.65 mr where q = 0, 1, 2,..., the far-field spot had two lobes; at angles of $(2q + \frac{3}{2})$ 1.65 milliradians the spot had one lobe. When reflector "D" was rotated to an angle just midway between these stable-mode alignments, slow oscillation between the modes was again observed (with beats at 19.67 MHz during the transition).

A set of beat frequencies at 17.22 MHz, 34.56 MHz, and 51.67 MHz was found at seven random positions of the roof-

edge of reflector "C" between 0.15 mm below its aligned position to 0.4 mm above. The frequencies did not change as the roof edge was adjusted in vertical position, but could be tuned over ±2 MHz, ±4 MHz, and ±6 MHz respectively by tipping the roof in horizontal alignment; the beats were most stable and had the highest amplitude at the midpoint of their tuning range. Since this set of frequencies were produced at each of the random positions simply by adjusting the alignment, it is assumed that the modes which produced them are supported by the resonator throughout the 0.55 mm position range.

The sensitivity of the peak far-field intensity to misalignment of reflector "C" was measured as $\delta\Phi = \pm 0.87$ mr. The output angle of this resonator was also fairly insensitive to alignment of the total reflector, changing by only 0.76 mr for each milliradion of reflector "C" rotation.

C ⊥ D Resonator, Au Position. With the roof edge of reflector "D" translated to the position which maximized the brightness of the orthogonal output, and the roof edge of reflector "C" returned to its aligned position, the near-field of the orthogonal and axial output appeared as shown in Fig 36. The resulting far-field spots are shown in Fig 37. The peak intensity of the leftmost (orthogonal) spot in Fig 37 below was measured as $I_o = 4.63$ w-cm^{-2}, with a divergence of $\theta = 0.86$ mr. The intensity distribution included symmetric secondary maxima of amplitude equal to that of the secondary maxima of the function given by equation (32)

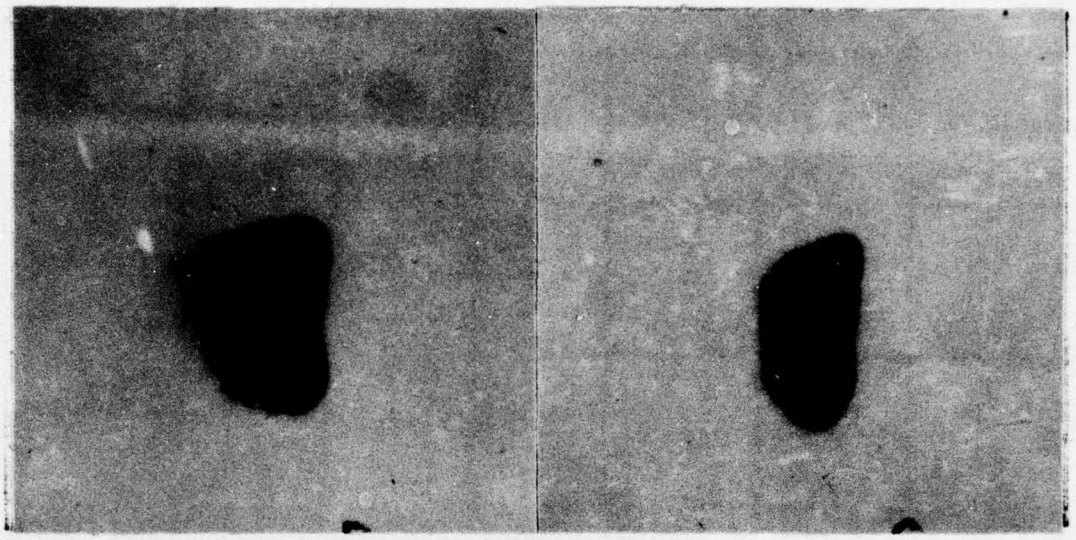

Fig. 36. Near-field thermo-fax burns of orthogonal and axial outputs of C⊥D resonator in Au position.

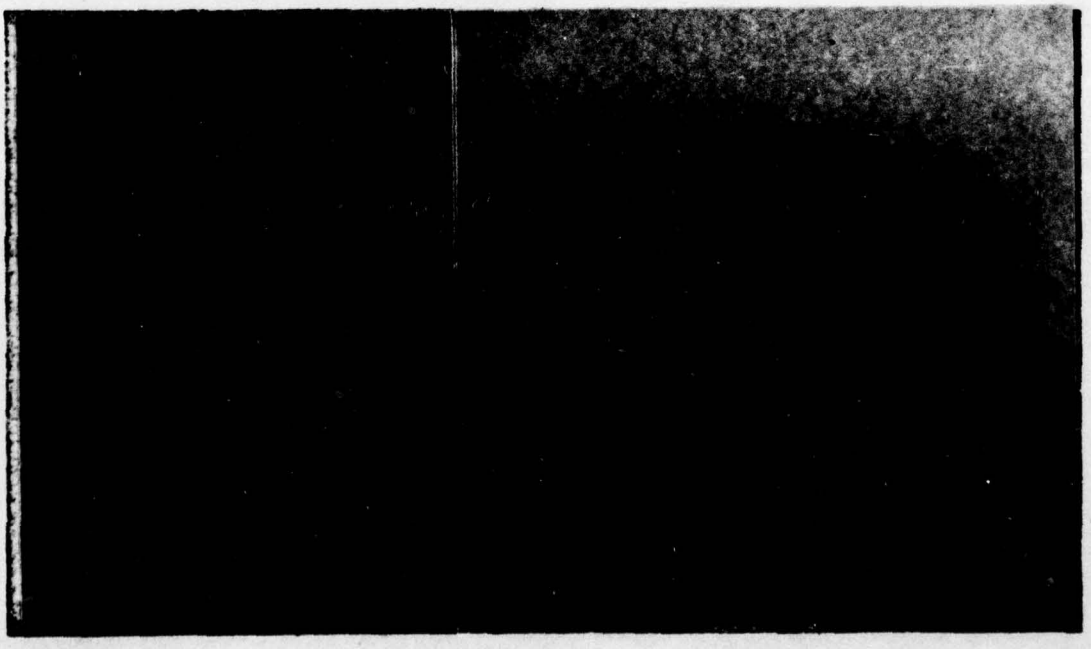

Fig. 37. Far-field orthogonal and axial spots from C⊥D resonator in Au position

(see chapter V), but which peaked about 1 mm further from the center than those of the theoretical Fraunhofer distribution. Fig 38 shows the intensity scan. A later measurement of the same parameters (after the cavity alignment had been changed and then returned to the aligned, Au position) showed secondary maxima slightly unsymmetric, but of approximately the same amplitude. Intensity and divergence were measured the second time as I_o = 5.07 w-cm^{-2} and θ = 0.93 mr.

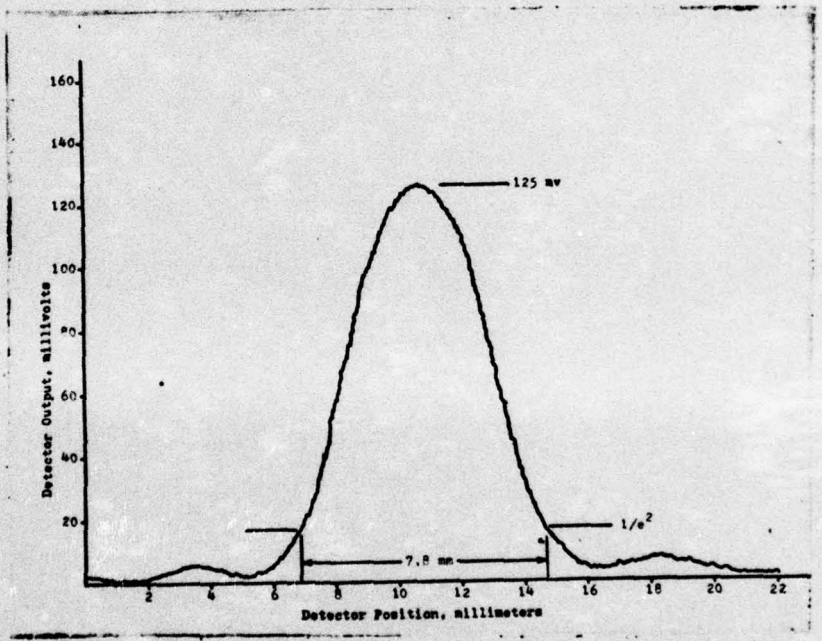

Fig. 38. Intensity at far-field of C_D, Au position

Translating the roof of the total reflector 0.5 mm above the axis produced a far-field spot with two lobes, vertically separated. A 19.33 MHz beat frequency was observed with the null of the spot centered on the detector.

Translating the roof to 0.3 mm above the axis produced a multimode output with beats at 17.9 MHz, 35.5 MHz, and

53.3 MHz. The linewidth and jitter of these beats were the same as all reported thus far (see chapter IV, Mode Beating).

The alignment sensitivity of intensity and beam output angle were respectively: $\delta\Phi = \pm 1.48$ mr and $\frac{\delta\theta}{\delta\Phi} = 0.73$.

C//D Resonator, M Position. The near-field and far-field spots from this configuration appeared identical to those of the aligned C|D configuration. With reflector "C" aligned for maximum intensity, three separate measurements of peak intensity and divergence were made by scanning through the far-field spots. The results were
$I_o = 4.64$ w-cm^{-2}, 4.29 w-cm^{-2}, and 4.29 w-cm^{-2};
$\theta = 1.08$ mr, 1.10 mr, and 1.08 mr.

Beat frequencies were observed for this configuration at all positions of the total reflector roof edge from the axis to the 1.0 mm position. The frequencies occurred in sets, and selection between the sets was achieved by tipping the roof edge. As the alignment of the roof was adjusted, one set of frequencies appeared on the screen of the frequency analyzer, moved across their tunable range, and disappeared. As this set was nearing its limit of tunability (and its amplitude was decreasing), another set appeared at the opposite limit and began to move across the range of tunability. There were two distinct sets of beats; they are identified by the frequency positions they occupy when tuned for maximum amplitude and stability (at the center of their range of tunability). Set #1 contained beats of frequency 14.43 MHz and 28.83 MHz; Set #2 had 7.17 MHz

14.5 MHz, 21.67 MHz, and 28.87 MHz. When the sets appeared together, the first set was at the upper limit of its tunable range and the second set was near its lower limit. The limits of tunability for the sets were approximately equal, and amounted to ±20% of the center frequency of each beat. Thus, for instance, the nominal 14.5 MHz beats were observed at 11.5 MHz and 17.3 MHz when they appeared together. The beats of set #2 are shown in Fig 39 as they appeared on the SPA-3000 analyzer screen:

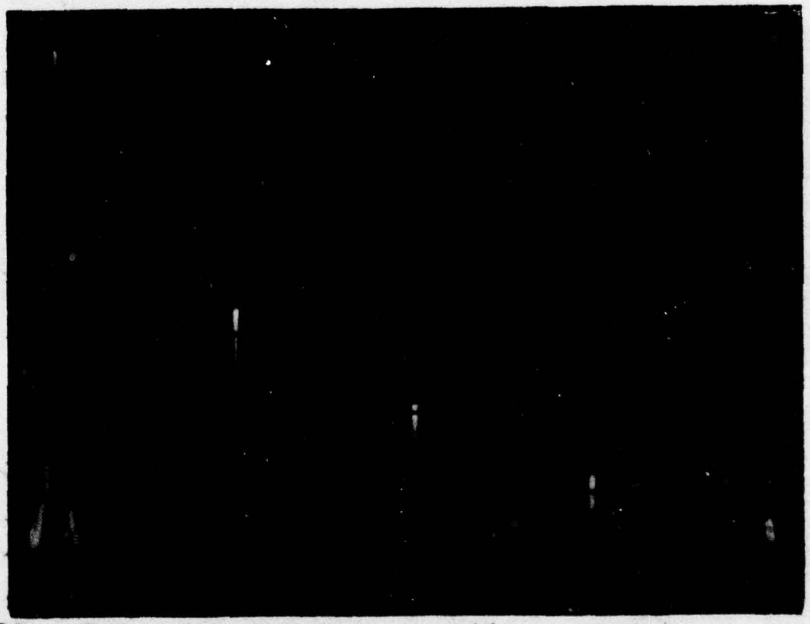

Fig. 39. Beat frequencies of C//D resonator, M position

When the position of reflector "C" was changed to 1.0 mm from the axis, a new set of beats was observed at 19.33 MHz and 38.33 MHz. No additional horizontal spreading of the far-field spot was apparent at this position, however.

Alignment sensitivity of intensity and output angle were measured as $\delta\Phi = \pm 0.42$ mr and $\frac{\delta\theta}{\delta\varphi} = 1.24$.

C//D Resonator, Au Position. With the output coupler translated to the position which optimized the brightness of the orthogonal outputs, the peak far-field intensity and beam divergence were I_o = 5.18 w-cm^{-2} and θ = 1.02 mr. The misalignment sensitivity was observed to be qualitatively the same as for the C//D, M position configuration.

C-D Resonator with Roofs Neither $\perp$ or //. The total reflector was rotated about the axis of the discharge tube while the laser was operating and the far-field spot was observed on the thermal screen. As expected, the alignment was found to be extremely critical as soon as the roof orientations deviated significantly from perpendicularity (ie, greater than a few degrees of rotation). Continual realignments were required to keep the output from being extinguished as the roof of "C" was rotated from horizontal to vertical.

Analysis

Effect of Output Coupler Position. The obvious improvement of intensity and divergence caused by translating the output coupler from position M to position Au is further evidence that its roof edge forms a limiting aperture with the inner edge of the (closer) discharge electrode. The close correlation of the far-field intensity distribution to that predicted for a plane wave passing through a rectangular aperture supports the hypothesis that the diffraction is mostly due to (nearly) vertical edges rather than circular holes.

Table V summarizes the far-field scan results for the aligned C⊥D and C//D Resonators:

Table V
Intensity and Divergence of C-D Roof Resonators

Roof Orientation	Output Coupler	I_o(w-cm^{-2})	Θ(mr)
Perpendicular	M	3.33	1.33
"	M	3.12	1.37
"	M	3.66	1.28
"	M	5.33	1.41*
"	M	3.18	1.33#
"	Au	4.63	0.86
"	Au	5.07	0.93
Parallel	M	4.64	1.08
"	M	4.29	1.10
"	M	4.29	1.08
"	Au	5.18	1.02

* superimposed axial and orthogonal outputs.
\# upper lobe only of two-lobe spot with "C" translated 0.6 mm from axis.

Comparing the intensity and divergence values obtained for the M output position with those measured while the coupler was in the Au position yields an interesting difference between the C⊥D and C//D configurations. Leaving out the two sets of results in table V to which the footnotes apply, and averaging the results taken under identical conditions yields the values of Table VI:

Table VI
Average Intensity and Divergence for Several C-D Resonator Configurations

Configuration	I_o (w-cm^{-2})	Θ(mr)
C⊥D, M	3.37	1.33
C⊥D, Au	4.85	0.90
C//D, M	4.41	1.09
C//D, Au	5.18	1.02

AD-A034 006 AIR FORCE INST OF TECH WRIGHT-PATTERSON AFB OHIO SCH--ETC F/G 20/5
AN EXPERIMENTAL INVESTIGATION OF THE RESONANT MODES OF A ROOFTO--ETC(U)
DEC 76 R L GROTBECK

UNCLASSIFIED GEP/PH/76-4 NL

2 OF 2
AD A034006

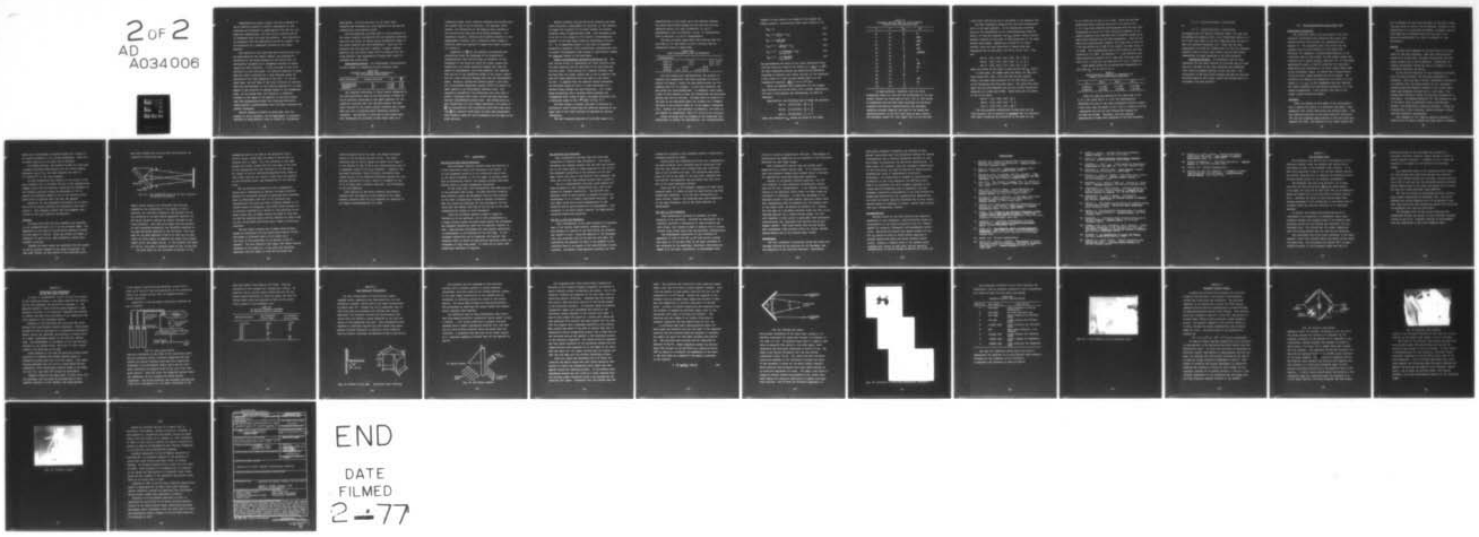

END

DATE FILMED
2-77

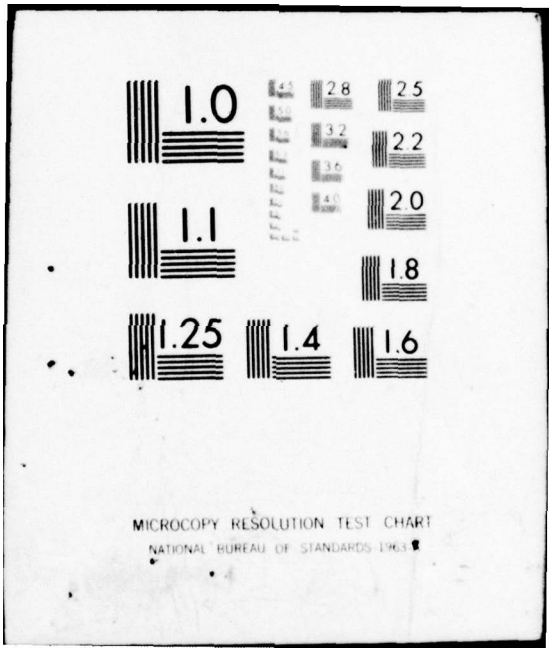
1.0
1.1
1.25
1.4
1.6
2.8
2.5
3.2
2.2
3.6
2.0
4.0
1.8
MICROCOPY RESOLUTION TEST CHART
NATIONAL BUREAU OF STANDARDS 1963-A

Translating the output coupler from the M position to the Au position produces a relative improvement in both intensity and divergence of approximately 45% when the roof edges are perpendicular, but only 17% in intensity and 7% in divergence when the roofs are parallel. This observation is consistent with the explanation offered in chapter V for the production of a plane-wave incident on the output aperture.

The fraction of the travelling wave reflected back into the gain medium by the output coupler, and subsequently diffracted by the narrow aperture on its return side, is horizontally elongated as it propagates through the medium toward the total reflector. If the roof edge of the total reflector is also horizontal, the effective aperture it makes with the (near) electrode has a long dimension along the direction of the long dimension of the wave. If, on the other hand, the roof edge of the total reflector is vertical, then the long dimension of the effective aperture is at right angles to the direction of maximum spread of the propagating beam. In the second case, the intensity of radiation incident on the edges of the aperture is very much higher than with perpendicular roofs; the resulting diffraction losses produce a proportionally lower far-field intensity and greater divergence.

Further analysis of Table VI shows that, with the coupler in the Au position, the 7% improvement in intensity achieved by using parallel roofs is offset by a 13% greater

beam spread. In the M position, on the other hand, intensity and divergence are both improved (by 31% and 22% respectively) with parallel roofs.

This is explained by noting that, in the M position of the output coupler, the aperture for the radiation reflected back into the cavity is larger and so diffraction losses at the total reflector are less significant. Since all the apertures are the same size, however, a larger combined aperture (for the cavity round trip) is obtained with the roofs parallel (and consequently a larger mode volume is available per round trip).

Misalignment Effects. The misalignment data presented in this chapter is summarized in the following table:

Table VII
Intensity and Output Angle Sensitivity
to C-D Resonator Misalignment

Roof Orientation	Coupler Position	$\delta\Phi$	$\frac{\delta\theta}{\delta\varphi}$
Perpendicular	M	± 0.87	0.76
Perpendicular	Au	± 1.48	0.73
Parallel	M	± 0.42	1.24

The observed differences in $\delta\Phi$ are easily understood in the same qualitative terms as the differences of Table VI: the Au position established a very small aperture for the radiation reflected back into the gain medium; the beam which returned to the output coupler therefore had a large spot size and a relatively small transverse intensity variation. The position of this spot on the output aperture determined the intensity of the output beam, so a

relatively larger total reflector alignment was allowed when the coupler was in the Au position. For parallel roofs, however, the diffraction by the aperture was a minimum in the direction the beam spot moved during alignment. Its transverse intensity variation was therefore greatest in the misalignment direction, and a relatively small change in reflector angle was required to change the output intensity by a factor 2.

Comparison of $\frac{\delta\theta}{\delta\varphi}$ for the parallel and perpendicular orientations shows the advantage of the crossed-roof configurations: when the roof edge of reflector "C" was misaligned in the plane for which the output coupler was insensitive, the output direction changed less than the amount of misalignment; with roofs parallel, the misalignment was not in the insensitive plane of the output coupler and the output direction changed more than the misalignment angle. Actually, diffraction effects played a role here, too, by providing significant energy (within the cavity) at small angles to the (misaligned) resonator axis. The (angularly insensitive) roof-reflectors were then able to select a high-gain path closer to the tube axis than geometrical considerations would allow. Had diffractions not been significant (ie, with larger apertures), the values of $\frac{\delta\theta}{\delta\varphi}$ for perpendicular roof orientation would have been unity (and $\frac{\delta\theta}{\delta\varphi}$ for parallel roofs might not have been measureable, since walkoff losses for this orientation are the same as for plane mirrors).

Besides changing the peak far-field intensity and beam output direction, misalignment of reflector "C" was observed to change the frequency of the beats between the several resonator modes by approximately ±20%. This phenomena seems to be due to the changes in the relative "interferometric lengths" of the mode paths caused by misaligning reflector "C". It is apparently unique to this type of alignment-insensitive resonator, since conventional configurations will not permit misalignments large enough to significantly change the relative lengths of the mode paths.

Effect of Translating the Roof of Reflector "C". The most obvious effect of translating the total reflector from its axial position was the splitting of the far-field spot into two lobes. This occurred at a smaller distance from the axis when the output coupler was in the Au position than when the output apertures were the same (0.5 mm versus 0.6 mm). It appears that the observed pattern represents the far-field output of the m = 1 mode travelling in a vertical plane between the roof reflectors. (ie, a mode whose projections onto a vertical plane resembles the "fundamental mode" drawn in Fig 5, but whose projection onto a horizontal plane is the "n^{th} mode" of Fig. 10.)

Off-axis energy to sustain this mode is provided by diffraction, which occurs when the effective aperture at the upper side of the total reflector is narrowed by vertical translation.

The beat frequency measured at 19.33 MHz seems to be

characteristic of this mode, as it was observed whenever the cavity was aligned between the two-lobe and one-lobe operating points (ie, C⊥D, M position, 0.3 mm "C" displacement; C⊥D, Au position, 0.5 mm "C" displacement; C//D, M position, 1.0 mm "C" displacement).

The sets of stable beats which were observed when the roof edge of "C" was within 0.3 mm of the axis had the frequencies listed in Table VIII:

Table VIII
Beat Frequencies of the C-D Resonator

Configuration						
C⊥D, M			17.2		34.6	51.67
C⊥D, Au			17.9		35.5	53.3
C//D #1		14.43		28.83		
C//D #2	7.17	14.5	21.67	28.87		

For the crossed-roof configurations, the analysis is slightly more complicated than that performed for the F-D results in Chapter V (where the mode paths between the F-D elements were all in a plane). In the C⊥D resonator, the mode paths are three-dimensional. To designate these modes, a pair of mode numbers is used, one identifying the horizontal pattern and one the vertical. The path which is parallel to the axis in the horizontal plane but projects as a fundamental mode in the vertical plane is, as an example, designated (10). Because the C⊥D resonator is symmetric, the order of the numbers is unimportant; Thus (10) and (01) are identical.

Since the modes must be in-phase at the reflectors (for diffraction to sustain the oscillation), the "interferometric

lengths" of each mode is the length of its longest leg. Simple geometric considerations show these lengths to be:

$$D_{00} = L \tag{33}$$

$$D_{01} = L \left(\frac{1}{\cos \alpha}\right) = D_{10} \tag{34}$$

$$D_{11} = L \left(\frac{1}{\cos \alpha\sqrt{2}}\right) \tag{35}$$

$$D_{02} = L \left(\frac{1}{\cos 2\alpha}\right) = D_{20} \tag{36}$$

$$D_{12} = L \left(\frac{1}{\cos \alpha\sqrt{1^2+2^2}}\right) = D_{21} \tag{37}$$

$$D_{22} = L \left(\frac{1}{\cos \alpha\sqrt{2^2+2^2}}\right) \tag{38}$$

By approximating the value of the cosine expression above with the first two terms of the series (ie, $\frac{1}{\cos \alpha} \approx 1 + \frac{\alpha^2}{2}$), the beat frequencies between the modes can be determined according to equation (26) (where now each of the subscripts m and p refer to a pair of mode numbers and f_o is the fundamental frequency: $\frac{qc}{2n_oL} \approx 2.83 \times 10^{13}$ Hz).

Since the measured beat frequencies for the aligned C|D resonator are in the ratio 1:2:3, several combinations of m and p could explain the observations, as Table IX indicates.

Specifically, the following sets of modes are possible:

Set A: (11)(01)(02) : $\frac{1}{2}$, 1, $\frac{3}{2}$

Set B: (11)(12)(02) : $\frac{1}{2}$, 1, $\frac{3}{2}$

Set c: (11)(22)(02) : 1, 2, 3

where the respective k_{mp} values are shown to the right.

Table IX
Frequency Ratios, kmp, for Beats Between
Various Three-Dimensional Modes

m	p	k_{mp}	set
01	00	$\frac{1}{2}$	FG
11	00	1	EFGH
11	01	$\frac{1}{2}$	ADFG
02	00	2	EFH
02	01	$\frac{3}{2}$	ADF
02	11	1	ABCDEFH
12	00	$\frac{5}{2}$	
12	01	2	D
12	11	$\frac{3}{2}$	BDI
12	02	$\frac{1}{2}$	BD
22	00	4	E
22	01	$\frac{2}{2}$	
22	11	3	CEI
22	02	2	CE
22	12	$\frac{3}{2}$	I

It seems probable, therefore, that the three dimensional modes (11) and (02) are oscillating in the C⊥D cavity; whether the third mode is (01), (12) or (22) cannot be determined from the data taken (although the far-field intensity distribution observed during this multimode operation strongly suggests that most of the energy was axially-directed, so the (01) mode would be more likely). The necessary values for "roof angle" are 1.11 mr for sets

A and B and 0.786 mr for set C, according to the equation (30).

The beat frequencies measured for the C//D configuration yield to the same analysis. If the frequencies resulting from all the combinations of the three-dimensional modes of order 2 or less are computed, the k_{mp} factors thereby derived provide a measure of the ratio of the frequencies of the beats between those modes. Making use of Table IX for these factors, there are only three sets of modes whose beat frequencies are in the ratio 7.25: 14.5: 21.75: 29.0. They are:

Set D: (01), (11), (12), (02) : $\frac{1}{2}$, 1, $\frac{3}{2}$, 2

Set E: (00), (11), (02), (22) : 1, 2, 3, 4

Set F: (00), (01), (11), (02) : $\frac{1}{2}$, 1, $\frac{3}{2}$, 2

where the series on the right of each set are the k_{mp} values.

In this case, the common modes are again (11) and (02). Since modes (00), (01), (12), and (22) are all equally likely, the exact mode structure of the C//D cavity could not be determined from this data above. The other data which exist for the C//D resonator are the set of beat frequencies observed at 14.5 MHz and 29 MHz. These beats are the result of one of the sets:

Set G: (11), (00), (01) : $\frac{1}{2}$, 1

Set H: (11), (00), (02) : 1, 2

Set I: (12), (11), (22) : $\frac{3}{2}$, 3

The nine possible combinations of mode sets for the C//D resonator can be resolved by <u>assuming</u> that the effective roof angle introduced by diffraction is the same for the

D, E, F sets as for the G, H, I sets. Since the two beat frequencies which resulted from one of the sets of the G, H, I type were observed simultaneously with the four beat frequencies of the D, E, F set, whichever alignment of the cavity existed at the time must have diffracted energy at an angle which produced all six beat frequencies. When all six beats were simultaneously present, the lower mode of the G,H, I set was shifted up by 20% of its nominal 14.5 MHz value to 17.3 MHz. The corresponding mode of the D,E,F set was then observed at 11.5 MHz. By equation (3?), the effective roof angle required to produce an 11.5 MHz beat from mode sets D and F is $\alpha = 0.6375$ mr; for mode set E it is $\alpha = 0.4508$ mr.

These angles yield the following beat frequencies for the lower k_{mp} of the sets G, H, I:

Table X
Beat Frequencies Inferred by Assumption of Single α for Simultaneous Mode Sets

α	Set G	Set H	Set I
0.6375 mr	5.75 MHz	11.5 MHz	17.25 MHz
0.4508 mr	2.87 MHz	5.75 MHz	8.63 MHz

Since 17.3 MHz was observed as the lower mode of the G, H, I set (when the D, E, F set was simultaneously operating) and none of the other frequencies listed in Table X were seen, only the modes of set I (at $\alpha = 0.6375$) could be responsible for the two beat frequencies centered at 14.5 MHz and 29 MHz. Therefore, only two possible combinations of modes were operating in the C//D resonator:

D + I: (12)(01)(11)(02) + (12)(11)(22)

or

F + I: (00)(01)(11)(02) + (12)(11)(22)

By dropping the two "axially directed" modes, (01) and (02) and adding the symmetric (22), set D transitions easily to I. Set F must lose three of its four modes and gain two more to make the observed transition to I. Since all the beat frequencies of a mode set blinked onto (or off) the frequency analyzer screen at once, sets D and I are the most likely combinations of modes operating in the C//D resonator.

Unexplained Effects. No explanation has yet been formulated for the beats observed at 19.33 MHz and 38.33 MHz when the roof-edge of the total reflector was translated "far" from its aligned position on the tube axis. The fluctuation of the C|D output between one-lobe and two-lobe far-field spots as the output coupler was rotated about its roof-edge is an open question.

VII. Two Reflectors With Roof Angles <90°

Experimental Conditions

The conditions under which this phase of the roof-resonator investigation was conducted were those which prevailed during the flat-90° roof experiments (see Chapter V). The exceptions were: the cavity flat was replaced with a total reflector of roof angle <90°, Reflector "E" (Appendix C contains specifications of the reflectors used in this study); the 90° output coupler was replaced with a Towles coupler, reflector "G", of roof angle approximately equal to that of reflector "E"; far-field diagnostics were performed on the axial output rather than on the orthogonal output, as before; and a concave mirror of 492 cm focal length replaced the 453 cm mirror. The reflector roof angles were nominally 2 mr (which is in the range $\alpha_o < \alpha < \alpha_m$), so the fundamental mode was expected. The cavity radiation was horizontally polarized, so it was always perpendicular to the vertical roof edge of the output coupler during this phase.

Variables

Since the purpose of this phase of the investigation was to examine the effect of a different roof-angle, fewer parameters were varied than during the previous phase. Only the transverse position of the total reflector (reflector "E") and its alignment angle relative to the tube axis were changed this time. The position of the output coupler was

set to maximize the far-field intensity of the axial output; this was found to occur at the Au position, contrary to the observations of the previous two phases. Likewise, the two roof edges were orientated about the tube axis to be mutually perpendicular (ie, roof of reflector "E" was horizontal).

Results

Two weak spots appeared in the far-field of the axial output of the E|G resonator. They were vertically separated by 25 mm and had a circular cross-section when the output coupler was in the Au position. Translating the coupler horizontally caused the spots to elongate in the horizontal direction, as before.

As the roof of reflector "E" was translated vertically from its axial position, the two spots alternated in intensity. There was also a slower, spontaneous alternation in intensity with the window heaters on (ie, turbulence induced around the Brewster windows) or for a short while after some parameter had been set to a new value. The steady-state condition tended to have equal intensities in both spots. By aligning reflector "E", the intensity of one of the spots could be maximized; after a few minutes, however, the steady-state condition prevailed. During the alternations of spot intensity, however produced, neither spot was completely extinguished.

The alignment of "E" could be carefully adjusted to cause one of the spots (usually the upper spot) to suddenly

break into a horizontally elongated smudge for a second or two before returning to its circular appearance. When this occurred, only one of the spots was so affected.

The HgCdTe detector was scanned through the lower spot to measure intensity distribution with the cavity aligned. Divergence was 1.3 mr, but peak intensity was down to 0.11 watts-cm^{-2} at the best alignment.

No beat frequencies were observed in the output of the E|G resonator (out to 100 MHz) for any of the configurations studied, except that the detector output was not displayed on the frequency analyzer during the adjustment of "E" to produce the momentary smudge of one of the far-field spots. Beats would be expected while the spot was smudged.

Reflector "E" was misaligned horizontally by an amount $\delta\Phi = \pm 0.84$ mr without reducing the intensity by more than a factor 2. This compares closely with the alignment sensitivity of the C|D resonator (M position).

Analysis

It seems clear that the E|G resonator was operating in its fundamental mode (m = 1) in the vertical plane. The separation of the spots in the far-field implies an effective roof angle of 2.54 mr. Since the actual roof angle of reflector "E" was 2.19 mr, some diffraction effects were probably occurring.

Because the axial output was optimized with the coupler in the Au position instead of the usual Ge position, the last pass through the gain medium in the horizontal plane

must have crossed the tube axis near the electrode, as output #1 in Fig 40 has done:

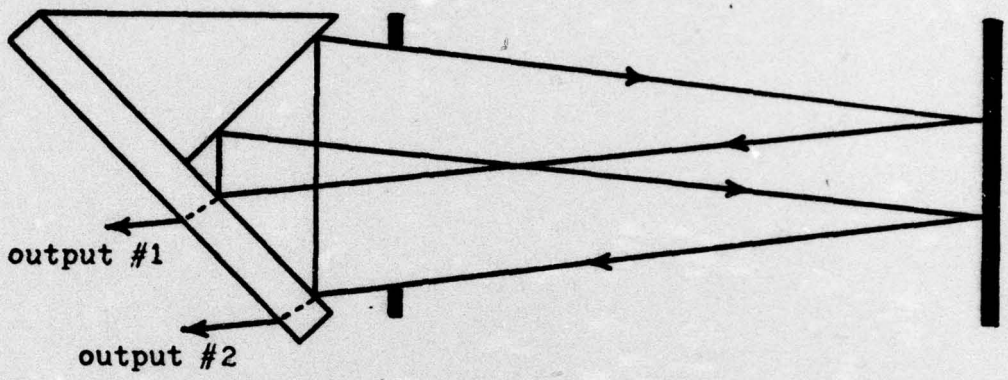

Fig. 40. The fundamental mode of the E⊥G resonator (horizontal projection)

Output ray #2 (nearest the electrode) was obviously degraded by the translation of the coupler to the Au position; the resultant widening of the aperture for the ray returning to the gain medium apparently improves output ray #1 enough to provide an overall increase in far-field intensity. Note that both output rays are parallel in this horizontal projection, and therefore transform to the same horizontal position in the far-field. Note also that the ray path depicted in Fig 40 is that for the edge limit; an entire family of parallel ray paths exist between output ray #1 and output ray #2. At the inferred roof angle of 2.54 mr, this band of parallel paths is only 2.6 mm wide.

The path drawn for the horizontal projection of the

fundamental mode is the same as its projection onto a vertical plane, except that the sense of Fig 40 must be inverted left to right. (ie, the reflector on the right becomes the output coupler with its roof edge in the plane of the drawing and the total reflector is on the left.) The origin of the two vertically-separated output beams is then clear: they are the result of rays which are parallel in the horizontal plane, and antiparallel in the vertical plane.

The low far-field intensity of this configuration arises from a combination of factors: the small effective aperture of the system produces an optimized beam divergence which is 40% greater than that of the optimized C|D configuration (and since far-field intensity depends on the inverse square of divergence, this effect alone accounts for an intensity reduction by a factor 2); the splitting of the axial output into two beams reduces the power of each lobe to half the combined output; and the reduction in mode volume (to the 2.6 mm bundle mentioned above) causes an additional reduction.

The ray bundle actually has a cusped cross section, caused by interaction with the curved inner surface of the electrodes on alternate sides of the bundle (as a ray trace of two round-trips of the pattern of Fig 40 reveals). For this effective roof angle, the widest vertical dimension of the bundle is 2.6 mm; since the electrode apertures clip the bundle in both the horizontal and

vertical projections of the mode, the widest horizontal extent of the ray bundle is also 2.6 mm. The cross-sectional area of such a cusped ray bundle (with cusps of 5.5 mm radius) is only 27.3% of the cross-sectional area of a comparable bundle in the C⊥D resonator. Together, the increased divergence, double outputs, and smaller mode volume account for an intensity difference between the C⊥D and E⊥G resonators of only a factor 15 (compared to the 30 to 40 times lower intensity observed). The discrepancy is not yet explained.

This analysis of far-field intensity distribution, together with the absence of mode beating in the output, strongly indicates that the E⊥G resonator is operating in the single three-dimensional (11) mode.

VIII. Conclusions

The 90° Roof-Flat Mirror Resonator

This multimode resonator embodies some bad features of a flat Fabry-Perot cavity and introduces a few others. It is very alignment sensitive in all directions except those in the plane orthogonal to the roof edge, is strongly dominated by diffraction effects, and supports several high-order spatial modes at various propagation directions.

On the other hand, this configuration does make good use of the available mode volume. Its peak far-field intensity with optimized output was 8% greater than the best produced by the other configurations (though at greater divergence). When the output was optimized for best divergence, the far-field spot was smaller than that of all but one of the other configurations (though at lower intensity).

Since the multimode operation seems to depend on diffraction by the apertures, use of this configuration in a higher Fresnel number structure might improve the divergence. The alignment sensitivity would not be improved, however; in fact, large-aperture structures will have greater sensitivity to misalignment in the direction of the roof edge. If its alignment sensitivity can be tolerated, the flat-90° roof resonator might be useful in applications requiring either low divergence or high total power. It would not be useful when single-mode operation is required.

The 90°//90° Roof Resonator

This configuration provided high far-field peak intensities at moderate beam divergences. (Its output divergence was somewhat greater than the best case studied due to the large number of modes supported in the cavity). The alignment sensitivity in the direction of the roof edge, better than that of the flat-90° roof resonator, was worse than the best case studied by more than a factor 3.

Use of a large-aperture structure would improve the beam divergence of this configuration also, but at the expense of alignment sensitivity. The 90°//90° roof Resonator would be best applied to systems for which the misalignment is in a single, predictable direction. The roof edges could then be both perpendicular to that direction and be quite insensitive to misalignment. This resonator is the worst choice, however, for applications requiring single-mode operation.

The 90° ⊥ 90° Roof Resonator

This configuration is the least sensitive to misalignment of the several cases studied, allowing nearly 3 milliradians of rotation of the roof before the intensity was reduced by half. Since the aperture of the discharge tube used subtended only 6.6 mr from the roof edge, the limitations was probably due more to the geometry of the structure than to the nature of the roof-reflector configurations. Providing a large-aperture structure for this

crossed-roof resonator would therefore produce a practically alignment-insensitive laser.

Output power was reasonably good from this configuration, the peak intensity (with optimized output) being down 9.3% from the best flat-90° roof intensity and only 2.1% below that of the 90°//90° roof case. The optimized beam divergence of 0.86 mr was equal to the best value obtained from the flat-90° configuration, and was better than that from any of the other resonators studied.

Since the 90° $\perp$ 90° resonator supported at least three separate modes, it cannot be used for applications requiring single-mode operation. It is the best configuration of those studied, however, for producing high peak intensities at low beam divergence, and is the least sensitive to misalignment.

The <90° $\perp$ <90° Resonator

This configuration produced an extremely low peak intensity in the far-field. Although the discrepancy can be partially ascribed to differences in beam divergence and mode volume, this resonator seems to operate with an intrinsically lower output power than the multimode configurations.

The misalignment sensitivity of this resonator is comparable to that of the 90° $\perp$ 90° roof cavity; because this angle is of the same order as the angle subtended at the reflectors by the apertures, structural limitations are judged to be the major contribution to misalignment sens-

itivity of mutually perpendicular <90°roofs. Misalignment of (practically) any magnitude can be tolerated if the (effective) apertures are made large enough.

This configuration was the only one studied which supported only a single spatial mode. It is therefore the only roof-resonator (among those studied) which is suitable for applications requiring single-mode operation.

Because of its greater inherent stability, the <90° roof resonator is less influenced by diffraction effects than the 90° roof configurations. It is, however, severely limited by the apertures, which reduce its mode volume and contribute to divergence. To take full advantage of the available volume in the gain medium, practical lasers using this configuration must be designed with roof angles close to the corner limit, as defined by equation (3). Because the roof edge of a two-plane reflector forms one side of the limiting aperture for a corner-limited design, the <90° roof resonator is best suited to gain media with rectangular cross-sections (eg, transverse flow devices such as gas-dynamic lasers). This would insure that the ray bundles have rectangular cross sections within the cavity, thereby making maximum use of the available gain volume.

Significance

The roof resonators investigated during this study were strongly affected by the structure of the discharge tube, and especially by the electrode aperture. Nonetheless,

sufficiently detailed information was obtained to draw general conclusions about the differences between the various configurations and to identify parameters peculiar to each which might be significant for particular applications. It seems clear, for instance, that true alignment insensitivity (in all directions) can only be achieved by using mutually-perpendicular roofs in large-aperture structures. Furthermore, the predictions of chapter II concerning mode instability in 90° roof resonators (the $n^{\underline{th}}$ mode limit) seem to be fulfilled; the <90° resonator operating in the corner-limited fundamental mode is apparently the only alignment insensitive configuration of the kind suitable for single-mode applications (eg, communications applications, for which the narrow observed linewidths may be very useful). Careful design is necessary to achieve usable power outputs with this configuration, however.

Recommendations

Further studies of the mode structure and operating parameters of roof resonators should certainly include an investigation of the effect of aperture size (ie, Fresnel number) on intensity, divergence, and misalignment sensitivity. Reflectors of various roof angles between 90° and 90° $-\alpha_o$ should be tried to verify stable operation of several higher-order modes (as theory predicts should occur). Finally, a careful study of the optimum output coupling ratio should be made under various operating configurations to provide design guidelines for future use.

Bibliography

1. Bobroff, D.L. "Modes of Optical Maser Cavities with Roof-Top and Corner-Cube Reflectors." Applied Optics, 3: 1485-1487 (December 1964).

2. Born, M. and E. Wolf. Principles of Optics (Fifth Edition). Oxford: Pergamon Press, 1975.

3. Checcacci, P.F., R. Falciai, and A.M. Scheggi. "Ring and 90° Roof Open Resonators." Proceedings of the IEEE (Letters), 62: 1611 L-1612L (November 1974).

4. Cheo, P.K. "CO_2 Lasers" in Lasers (Vol. 3), edited by A.K. Levine and A.J. DeMaria. New York: Marcel Dekker, Inc., 1971.

5. Chun, M.K., and E.A. Teppo. "Laser Resonator: An Electrooptically Q-Switched Porro Prism Device." Applied Optics, 15: 1942-1946 (August 1976).

6. De Lang, H., and G. Bouwhuis. "A Gas Laser with a Non-Degenerate Configuration of Three Plane Mirrors." Physics Letters, 5: 48-50 (June 1963).

7. Deutsch, T.F. "Gain and Fluorescence Characteristics of Flowing CO_2 Laser Systems." IEEE Journel of Quantum Electronics, QE-3: 151-155 (April 1967).

8. Dunkle, J.E. A Study of the Reliable Generation of Zero π Pulses With a Mode Locked CO_2 Laser. Unpublished thesis. Wright-Patterson Air Force Base, Ohio: Air Force Institute of Technology, June 1973.

9. Eckbreth, A.C. "Coupling Considerations for Ring Resonators." IEEE Journal of Quantum Electronics, QE-11: 796-798 (September 1975).

10. Evans, H.E. The Geometric Theory of Roof Reflector Resonators. Unpublished thesis. Wright-Patterson Air Force Base, Ohio: Air Force Institute of Technology, October 1976.

11. Evans, H.E. Private communication.

12. Gerry, E.T., and D.A. Leonard. "Measurement of 10.6 μ CO_2 Laser Transition Probability and Optical Broadening Cross Sections." Applied Physics Letters, 8: 227 (May 1966).

13. Gould, G., et al. "Crossed Prism Interferometer." Applied Optics, 1: 533-534 (July 1962).

14. Heard, H.G. Laser Parameter Measurements Handbook. New York: John Wiley & Sons, Inc., 1968.

15. Kogelnik, H., and T. Li. "Laser Beams and Resonators." Proceedings of the IEEE, 54: 1312-1328 (October 1966).

16. Maitland, A., and M.H. Dunn. Laser Physics. London: North Holland Publishing Co, Ltd., 1969

17. Moeller, G., and J.D. Rigden. "High Power Laser Action in CO_2-He Mixtures." Applied Physics Letters, 7: 274-276 (November 1965).

18. Menegozzi, L.N., and W.E. Lamb, Jr. "Theory of a Ring Laser." Physical Review A, 8: 2103-2125 (October 1973).

19. Pasqueletti, F., and L. Ronchi. "Integral Equation for a 90° Roof Mirror Optical Resonator." Journal of the Optical Society of America, 64: 289-294 (March 1974).

20. Pasqueletti, F., and L. Ronchi. "Roof-Mirror Resonators." Journal of the Optical Society of America, 65: 649-654 (June 1975).

21. Powell, T. "The Design and Operation of a Modular Carbon Dioxide Laser System." Optics and Laser Technology: 19-23 (February 1972).

22. Ronchi, L. "Low-Loss Modes and Resonances in a Quasi-90°-Roof Mirror Resonator." Applied Optics, 12: 93-97 (January 1973).

23. Rothstein, J. "Isosceles Total Internal Reflectors as Optical Elements." Applied Optics, 2: 1191-1194 (November 1963).

24. Scheggi, A.M., P.F. Checcaccii, and R. Falciai. "Modes and Modes Degeneracy in 90° and Quasi-90° Roof Open Resonators." Journal of the Optical Society of America, 65: 1050-1053 (September 1975).

25. Siegman, A. An Introduction to Lasers and Masers. New York: McGraw Hill Book Co., 1971.

26. Soncini, G., and O. Svelto. "Single Transverse Mode Pulsed Ruby Laser." Applied Physics Letters, 11: 261-263 (October 1967).

27. Soncini, G., and O. Svelto. "Single Mode Passive Q-Switched Rube Laser." IEEE Journal of Quantum Electronics, QE-4: 422 (June 1968).

28. Toraldo di Francia, G. "Flat-Roof Resonators." Applied Optics, 4: 1267-1270 (October 1965).

29. Towles, P.M. Private Communication.

30. Weichel, H., and L.S. Pedrotti. "A Summary of Useful Laser Equations - An LIA Report." Electro-Optical Systems Design: 22-35 (July 1976).

Appendix A

The Discharge Tube

The discharge tube used for this investigation of roof-reflector resonant modes was designed and constructed by John Dunkle as part of his graduate thesis project. It is most fully described in Ref 8, but its more salient features are briefly described here to identify the limitations which the gain medium placed on the resonator performance.

The discharge tube was 15 mm ID Pyrex, 134 cm long. Into each end were fitted Pyrex $\frac{19}{38}$ ground glass points, 15 cm long; the outer end of each joint was cut at Brewster's angle and sealed with a 6 mm thick disk of optical quality Na Cl. Rotating the joints in their ground glass seats allowed adjustment of the orientation of the window plane of incidence while the tube was evacuated to its operating pressure.

To prevent the windows from deteriorating due to condensation (or absorption) of atmospheric water vapor, resistive heaters were wrapped around 10 cm diameter glass cylinders placed over the windows and concentric with the discharge tube. The heaters kept the window temperature near 37°C during periods when the tube was not operating.

The electrodes were 25 mm nickel cylinders, 11 mm inside diameter, which were polished smooth and snugly fitted inside the pyrex tube. The electrodes were spaced 128.7 cm apart center-to-center, so the discharge length was 126.2 cm.

Electrical power for the discharge was provided by a Universal Voltronics "Labtrol" supply through a series of ceramic ballast resistors. A maximum of 4 KW of power was available to be shared by the resistors and discharge plasma.

The constituent gases of the discharge medium entered the tube through ports near each end and were evacuated from a port midway between the electrodes, thereby maintaining a flow of cool gas over the electrode surfaces (Dunkle's system supplied gas to the center and pumped from the ends). The pump was a Welsh Duo-Seal, model #9080-97.

The tube was cooled by circulating tap water through a pyrex jacket surrounding the discharge tube. The entire assembly was rigidly supported on a 10 cm aluminum I-beam rail (onto which were also mounted the cavity roof-reflectors, the alignment flat, and the retro-flat).

The alignment axis for the cavity reflectors was established through the centers of both electrode cylinders (within ±1 mm) by an iterative rotation of the alignment flat and translation of the He-Ne alignment laser.

Appendix B

Contruction and Calibration of the Gas Supply Manifold

In order to independently control the partial pressure of the constituent gases, a gas supply manifold was constucted for the discharge tube described in Appendix A. The manifold permitted three different gases, supplied in high pressure K bottles, to be separately regulated and metered; it thereby provided fine adjustments of the composition and total pressure of the discharge medium.

Metering of the individual gas flow rates was accomplished with three Gilmont tapered flowmeters. These meters allowed the flow of each gas to be controlled by micrometer needle valves; the resulting flow produced a viscous force on a small, lightweight sphere in the vertical, tapered tube. The displacement of the sphere in the tube was proportional to the viscous force, which was, in turn, proportional to the flow rate of the gas.

Total pressure in the tube was monitored during normal operation by a Wallace and Tiernan pressure gauge (a mechanical Bourdon type with 0-50 torr range). Leak checking was performed with the aid of a Consolidated Vaccuum Corporation (CVC) thermocouple pressure gauge in the range 0-1 torr (ie, less than 1000 microns Hg equivalent).

Complete mixing of the gases prior to their entry into the discharge tube was aided by allowing them to flow together through a 2 liter chamber; the large diameter

of the chamber required the gas molecules to move with a lower drift velocity than they maintained in the connecting tubing, and thereby allowed time for adequate mixing by thermal agitation.

Components of the gas-supply system were assembled as Fig 41 depicts:

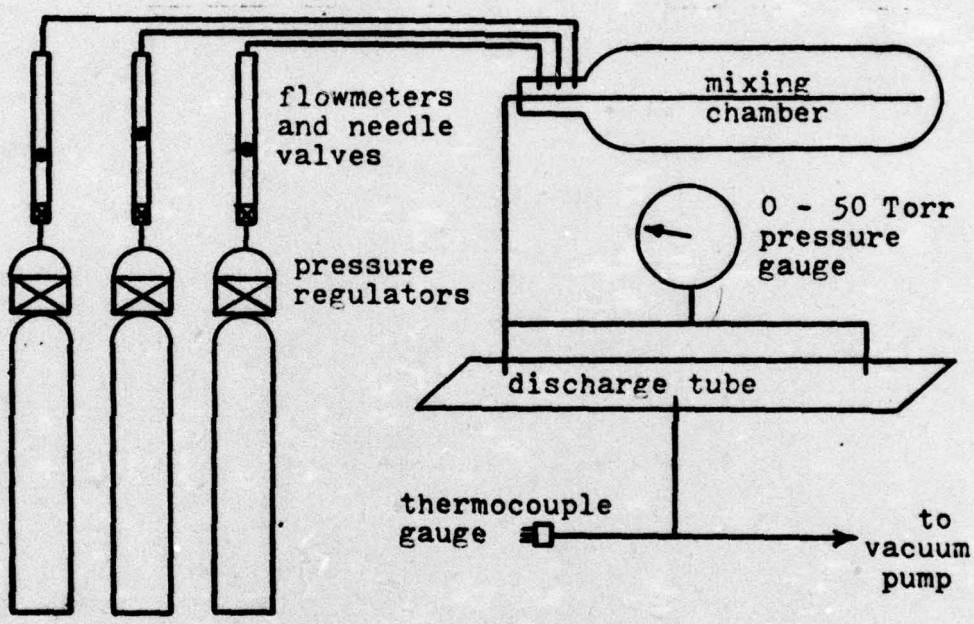

Fig. 41. Gas supply system

Absolute calibration of the flows of the constituent gases was not attempted; rather a relative comparison was made between the partial pressure resulting from a particular adjustment of the micrometer needle valves and the flowmeter indication so produced (read at the top of the flowmeter sphere). Table XII gives the comparison between these two parameters for the nitrogen and carbon dioxide flowmeters. The helium flowmeter was extremely unsteady and could not be calibrated (ie, the sphere oscillated in the

tube over ±10% of full scale at all flows. This was attributed to the extemely low viscosity of helium). In practice, the N_2 and CO_2 needle valves were set for the proper partial pressures of those two gases, and then the helium needle valve was adjusted to make up the correct total pressure in the discharge tube.

Table XI
N_2 and CO_2 Flowmeter Readings
at Various Partial Pressures

Partial Pressure	CO_2 Flowmeter, % full scale	N_2 Flowmeter % full scale
1.0 torr	12 %	10 %
1.5	18	15
2.0	23	17
3.0	29	25
4.0		31
5.0	34.5	
7.0	39	
8.0		40
10.0	46	43

Appendix C

Roof Reflector Fabrication

For this investigation of roof-reflector modes, resonant cavity components were fabricated with two flat reflecting surfaces, joined with a very small discontinuity at angles near 90°. Because the 10.6 μ wavelength used in this study does not propagate well through most optical materials, the reflector utilized the first-surface reflection from thin metallic layers deposited on the flat substrate of the supporting structure. This configuration was achieved by cementing together two gold-coated right angle prisms of proper dimensions to produce a solid reflector with an interior roof-edge (as depicted in Fig 42 and Fig 43.

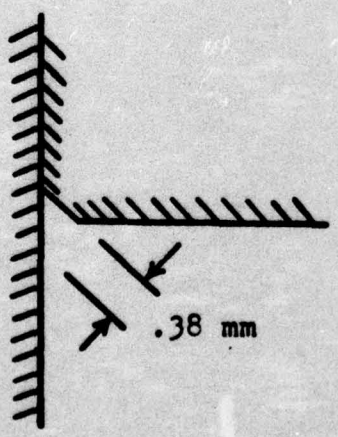

Fig. 42. Detail of roof edge

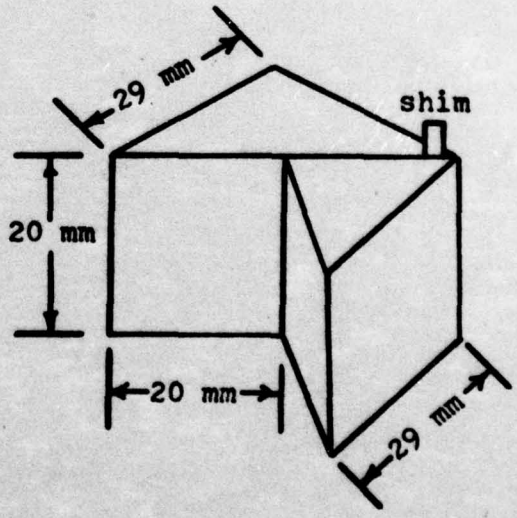

Fig. 43. The total reflector

This geometry has the advantage of flat mounting surfaces and no entrance surface to produce spurious reflections. Gold was chosen as the coating material because of its high (>99%) reflectivity in the infrared and its resistance to tarnishing during the course of the investigation. The exact angle between the reflecting surfaces was established by inserting thin shims between the elements before cementing them together.

The reflectors used in this investigation were fabricated from Edmund Scientific Corporation "better grade" prisms. (However, a 90° quartz prism with a chipped roof edge, salvaged from a broken cryptocynine Q-switch cell, was used for the first rooftop reflector until the prism order was received). A germanium flat was used for an output coupler in a technique suggested by Towles (Ref 29) and depicted in Fig 44:

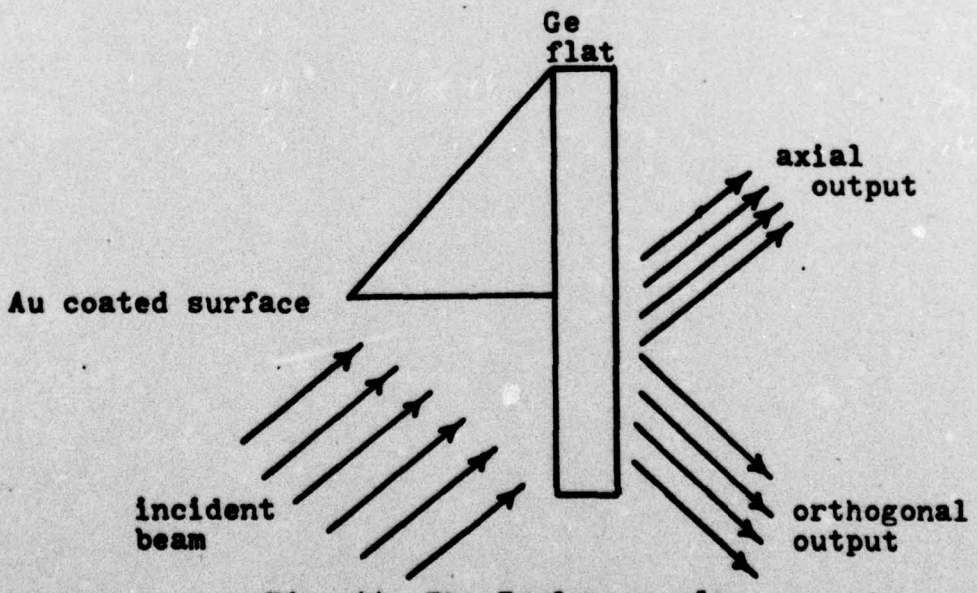

Fig. 44. The Towles coupler

The components were first meticulously cleaned with DeContam (a Kern Chemical Company detergent) and acetone to remove residual surface contaminants and grease. One of the reflector elements was supported on the work table with its reflecting surface horizontal. (Masking tape was occasionally used to mark the exact position of the second element on the horizontal surface). If required, shims of aluminum (.23 mm) foil, paper, and cellophane were placed on the horizontal surface parallel to the vertical roof edge. A drop of Duco cement was placed on a cotton swab (which had been saturated with acetone) and then sqeezed into the swab with the fingers until thoroughly dissolved in the acetone. More acetone was added to the swab to replace that lost by evaporation during the squeezing process, and a large drop of the resulting mixture was applied to the horizontal surface of the reflector components. The second reflector component was then placed carefully on the horizontal surface and the cement-solution drop squeezed out to the edges of the joint. Care was taken that the cement solution did not squeeze out past the roof edge onto the eventual reflecting surface.

After the cement had thoroughly set (>16 hours) the reflector was gently wiped with lens tissue saturated with acetone to remove any fingerprints which might have been applied during the cementing process. (A hot-ethanol-vapor degreasing process was once tried as a final cleaning step, but the Duco cement dissolved within a few seconds and the reflector fell apart. Thereafter only the acetone wipe was

used). The reflector was lifted with clean tongs and placed under a bell jar 10 cm from a coiled tungsten filament. Gold wire was placed on these heater coils and the bell jar was evacuated to 2×10^{-6} mm Hg. Current was supplied to the filament from an extended power supply and adjusted to maintain the temperature of the gold just above its melting point. In about 10 minutes enough gold had evaporated from the filament to deposit an optically opaque layer on the microscope slide (also 10 cm from the filament). The reflector was thus judged to be totally reflecting at infrared frequencies and was removed from the bell jar.

A collimated beam from a Spectra-Physics Model 132 He-Ne laser was directed onto the roof edge of the completed reflector and the reflected beam was analyzed to determine the angle α by which the roof angle deviated from exactly 90°. The reflected beam actually had two components as depicted in Fig 45. These components formed two distinct spots when focused to the far-field by a spherical mirror (984 cm radius of curvature); the separation of the spots, r, was then taken as a measure of the angle α according to the relation

$$\alpha = \frac{1}{4} \left(\frac{r}{492\ \text{cm}}\right) \text{ radians} \qquad (39)$$

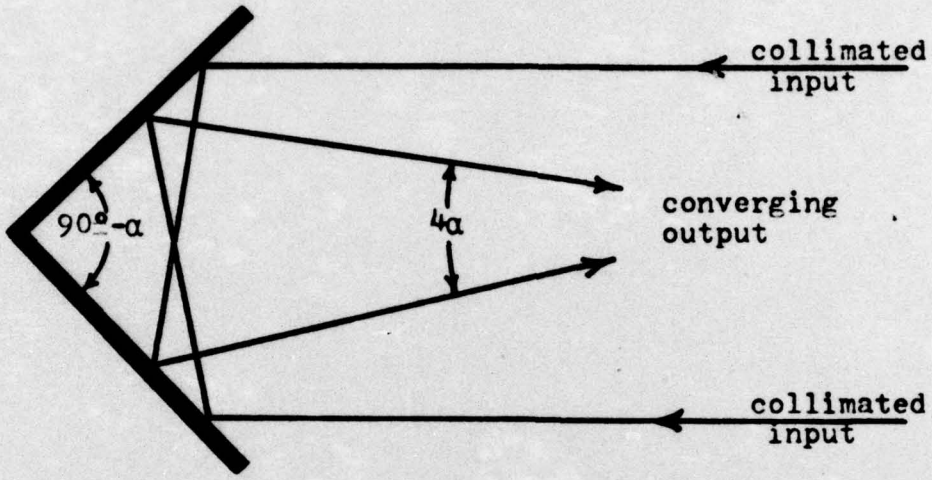

Fig. 45. Testing roof angles

With proper collimation of the input beam, (using a 10 X Gaertner telescope) the spots were focused to a diameter of the order of 1 mm. By allowing these spots to expose a bare piece of polaroid film placed in the focal plane, their separation was eventually determined to within 0.2 mm. The angle α was thereby determined (for the last several reflectors) within ±10 μr. The spots were also monitored during the assembly of the reflectors to adjust the shims. It was necessary to press the two parts tightly together while checking shim thickness since Duco cement shrinks as it dries and compresses the shims. The angle α was found to change by several hundred microradians as the cement hardened, making the reflector fabrication a lengthy trial-and-error process. Fig 46 shows the different appearance of

the spots as the technique evolved.

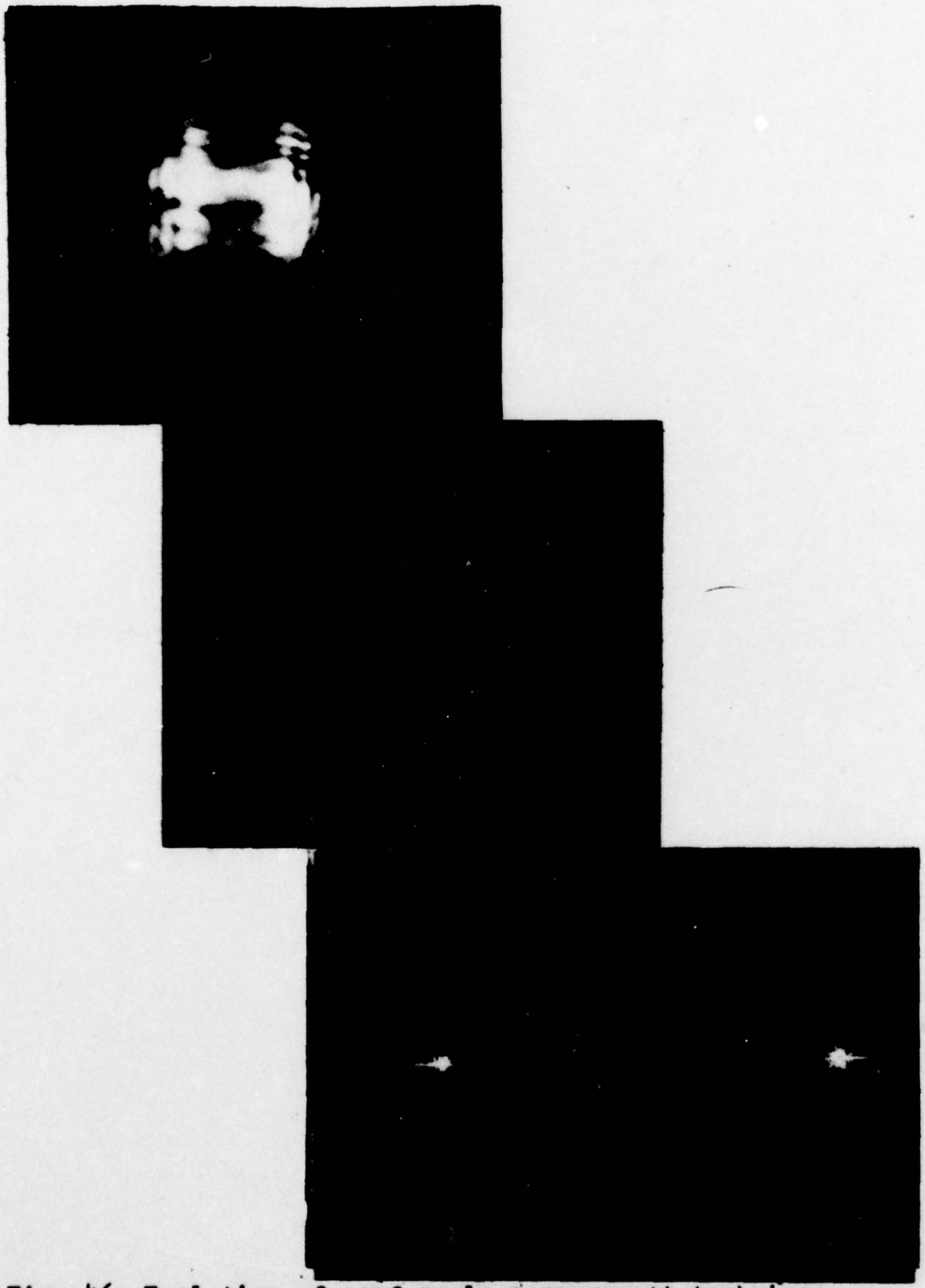

Fig. 46. Evolution of roof angle measurement technique.

The reflectors fabricated by the above technique and subsequently used as resonator elements in this investigation are listed in Table XII with their roof angles.

Table XII
Resonator Element Specifications

Reflector	Roof Angle, α	Type and Use
A	0°± 600μr	total reflector to set up diagnostics
B	0°± 250μr	not used (bad glue job)
C	0°± 125μr	total reflector for 90°-Roof study
D	0°± 25μr	output coupler for 90°-Roof study
E	2.19mr± 10μr	total reflector for <90°-Roof study
F	N/A	flat total reflector, 2 cm diameter
G	2.05mr± 10μr	output coupler for <90°-Roof study
H	.051mr± 10μr	output coupler for demonstration
J	.076mr± 10μr	total reflector for demonstration

The last two reflectors listed above were used to demonstrate the operation of a roof-reflector laser during a briefing for the Commander of Air University.
A completed roof reflector is shown in Fig 47.

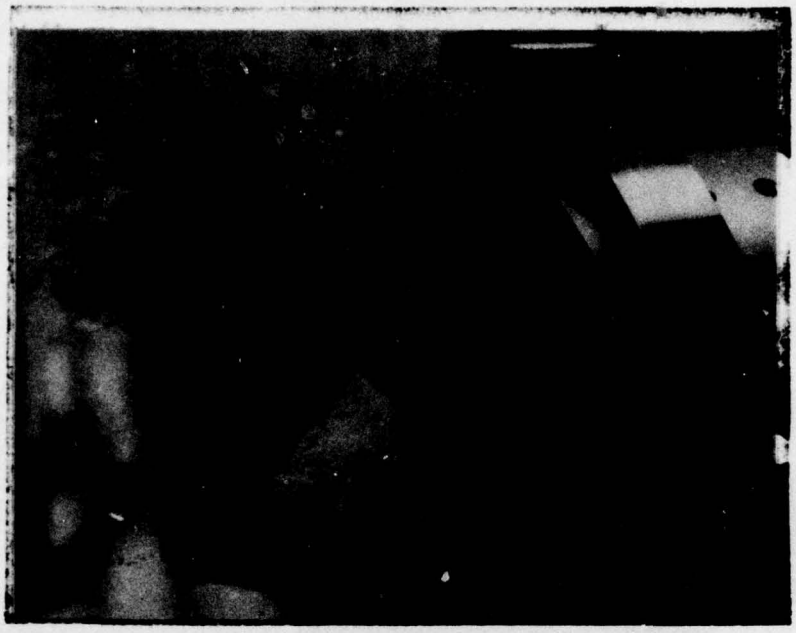

Fig. 47. A roof reflector on its adjustable mount

Appendix D

Intensity Scanner System

A system for detecting and recording the far-field intensity distribtions of the several roof-resonators studied was constructed and calibrated. The principal component of the system was a cooled (to 77°K) mercury-cadmium-telluride detector manufactured by Société-Anonyme de Télécommunications (Serial # 896, PL334). This detector, which had a sensitive area of $6 \times 10\text{-}4$ cm^2, was mounted in a metal dewar behind an anti-reflection coated germanium window. The spectral response of the detector peaked at 11.48 μ, whereas the window transmissivity was a maximum (96%) at 10.4 μ. The detectivity of the photoelectric element was

$$D^* = 3.7 \times 10^9 \text{ cm} - \text{Hz}^{\frac{1}{2}} - \text{w}^{-1} \text{ @ } 10.6\ \mu \text{ wavelength.}$$

In order to achieve maximum responsivity of the detector, it was operated in the photoconductive mode (rather than the photovoltaic mode). To avoid the difficulty of searching for millivolt signals superimposed on approximately one-volt D.C. bias, the detector was electrically connected as one leg of a resistive bridge network as diagrammed in Fig 48. This method of operation had several advantages: no capacitive coupling was necessary to block the bias voltage, so the frequency response of the system extended to true D.C.; the residual capacitance of the components was low enough that the high frequency response extended to the hundred-

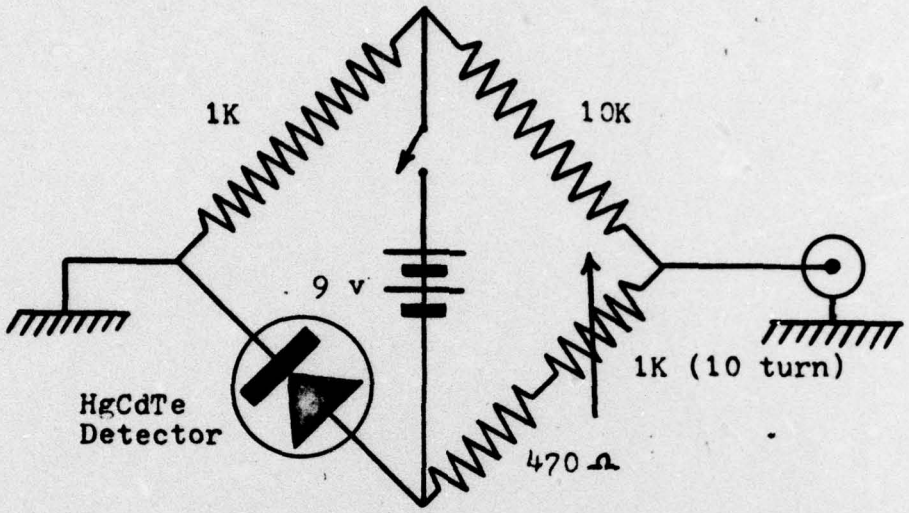

Fig. 48. Detector bias bridge

megahertz range; the variable resistance in the one leg of the bridge allowed the network to be balanced for the changing resistance of the detector as it responded to the occasionally varying infrared view through its window (a small point, to be sure, but extremely handy when looking for tiny signals). The completed circuit was installed in a mini-box and connected directly to the BNC output connector of the dewar assembly. Fig 49 shows the completed circuit. The detector dewar assembly and detector bias assembly were both mounted on a travelling micrometer stage to allow precise horizontal positioning of the sensitive area of the detector. A 5000 Ω linear potentiometer was fastened to the travelling stage and connected across the terminals of a 6 volt latern battery; its wiper potential was then propor-

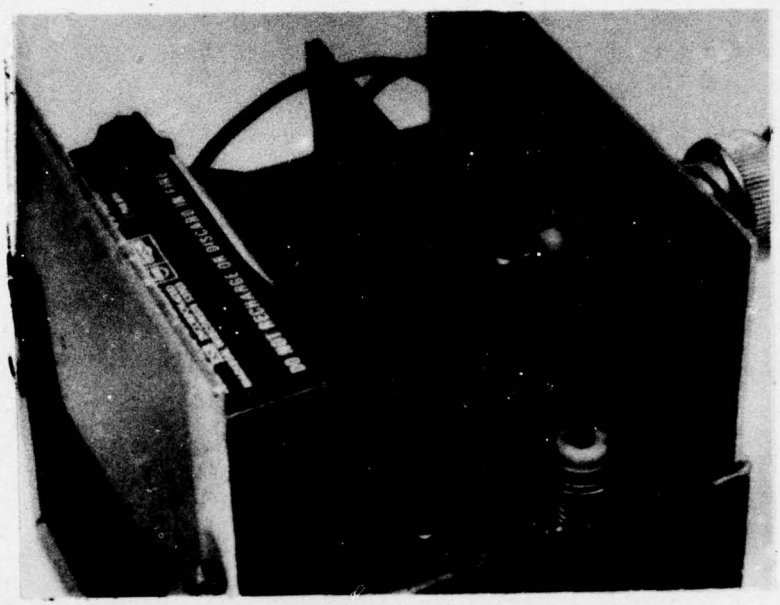

Fig. 49. Detector bias assembly

tional to the horizontal position of the detector, and was used as the horizontal input signal to an X-Y recorder.

The output of the detector bias network was amplified by a Kiethley Model 600A electrometer and used as the vertical input signal to the X-Y recorder. In this manner, a two-dimensional plot was obtained of intensity versus horizontal dimension of the far-field output beam of the roof resonators. The X-Y recorder amplitudes were calibrated against the travelling-stage micrometer readings and against the Keithley electrometer scale readings, respectively. Fig 50 shows the detector dewar, bias network assembly, and linear potentiometer mounted on the travelling stage:

Fig. 50. Intensity scanner

VITA

Ronald Lee Grotbeck was born on 11 March 1941 in Watertown, South Dakota. Raised in Bellevue, Nebraska, he was educated in a Midwestern environment through his graduation from the College of St. Thomas, St. Paul, Minnesota, in 1963. At that time he received the degree of Bachelor of Science in Physics and Mathematics and a Regular Commission in the USAF as a Distinguished ROTC Graduate.

Assigned immediately to the AF Weapons Laboratory at Kirtland AFB, he performed research on the operation of solid-state laser devices and their effect on various systems. He attended Squadron Office School with the class of 1967D. Upon returning to the Weapons Lab, he assisted in the design and fabrication of an advanced target designator and was a member of the evaluation team during combat tests at Con Thien, RVN, in 1968.

Assigned in 1969 to the Air Force Technical Applications Center in Washington DC, he spent three years designing optical diagnostic systems and analyzing their performance during several summer-long experiments in Hawaii.

Recalled to the AF Weapons Laboratory in 1972, he supervised the activities of the Optics and Data Analysis section at the Sandia Optical Range, performing high-power gas-dynamic laser experiments until his entry into the Graduate Engineering Physics program of the Air Force Institute of Technology in 1975.

UNCLASSIFIED

SECURITY CLASSIFICATION OF THIS PAGE (When Data Entered)

REPORT DOCUMENTATION PAGE	READ INSTRUCTIONS BEFORE COMPLETING FORM
1. REPORT NUMBER (14) GEP/PH/76-4	2. GOVT ACCESSION NO. / 3. RECIPIENT'S CATALOG NUMBER
4. TITLE (and Subtitle) (6) AN EXPERIMENTAL INVESTIGATION OF THE RESONANT MODES OF A ROOFTOP LASER.	5. TYPE OF REPORT & PERIOD COVERED: MS Thesis
	6. PERFORMING ORG. REPORT NUMBER
7. AUTHOR(S) (10) Ronald L. Grotbeck ~~Major, USAF~~	8. CONTRACT OR GRANT NUMBER(S) (9) Master's thesis,
9. PERFORMING ORGANIZATION NAME AND ADDRESS: Air Force Institute of Technology(AFIT-EN) Wright-Patterson AFB, Ohio 45433	10. PROGRAM ELEMENT, PROJECT, TASK AREA & WORK UNIT NUMBERS
11. CONTROLLING OFFICE NAME AND ADDRESS (11) Dec 76	12. REPORT DATE: December, 1976
	13. NUMBER OF PAGES (12) 138 p.
14. MONITORING AGENCY NAME & ADDRESS(if different from Controlling Office)	15. SECURITY CLASS. (of this report): Unclassified
	15a. DECLASSIFICATION/DOWNGRADING SCHEDULE

16. DISTRIBUTION STATEMENT (of this Report)

Approved for public release; distribution unlimited

17. DISTRIBUTION STATEMENT (of the abstract entered in Block 20, if different from Report)

18. SUPPLEMENTARY NOTES: Approved for public release; IAW AFR 190-17

JERRAL F. GUESS, Captain, USAF
Director of Information

19. KEY WORDS (Continue on reverse side if necessary and identify by block number)

Laser resonant modes
Rooftop laser
Alignment-insensitive laser
Cavity modes
Roof reflector
Laser mode measurement
Roof-mirror resonator

20. ABSTRACT (Continue on reverse side if necessary and identify by block number)

First-surface roof-reflectors were constructed with apex angles near 90 deg and used as resonator elements in a 2-meter laser cavity with a gain medium of electrically excited CO_2, N_2, and He at 10 torr pressure. The divergence, far-field intensity distribution, and beat frequency components were measured for the output beams of several roof-resonator configurations. Both single-mode and multi-mode operation was achieved, and the mode structure of the several alignment-insensitive configurations was inferred.

DD FORM 1 JAN 73 1473 EDITION OF 1 NOV 65 IS OBSOLETE

UNCLASSIFIED

SECURITY CLASSIFICATION OF THIS PAGE (When Data Entered)

012 225